Paradoxical mTORC1-Dependent microRNA-mediated Translation Repression in the Nucleus Accumbens of Mice Consuming Alcohol Attenuates Glycolysis

Yann Ehinger[1], Sophie Laguesse[1#], Khanhky Phamluong[1], Alexandra Salvi[1], Zachary W. Hoisington[1], Drishti Soneja[1^], Yoshitaka J. Sei[2], Ken Nakamura[1, 2] and Dorit Ron[1*]

[1] Department of Neurology, University of California, San Francisco, San Francisco, California, 94158, USA

[2] Gladstone Institute of Neurological Disease, Gladstone Institutes, San Francisco, California, 94158, USA

[#] Present address: S.L GIGA-Neurosciences, University of Liege, Belgium

[^] Present address: D.S Johns Hopkins University School of Medicine, Baltimore, USA

* Correspondence: D. Ron, Department of Neurology, University of California, San Francisco, 675 Nelson Rising Lane, BOX 0663, San Francisco, CA 94143-0663, USA. dorit.ron@ucsf.edu

Keywords: mTORC1, Translation, microRNA, Alcohol, Addiction, Striatum, Nucleus Accumbens, Glycolysis, Aldolase A, microRNA-34a

SUMMARY

mTORC1 promotes protein translation, learning and memory, and neuroadaptations that underlie alcohol use and abuse. We report that activation of mTORC1 in the nucleus accumbens (NAc) of mice consuming alcohol promotes the translation of microRNA (miR) machinery components and the upregulation of microRNAs (miRs) expression including miR34a-5p. In parallel, we detected a paradoxical mTORC1-dependent repression of translation of transcripts including Aldolase A, an essential glycolytic enzyme. We found that miR34a-5p in the NAc targets Aldolase A for translation repression and promotes alcohol intake. Our data further suggest that glycolysis is inhibited in the NAc manifesting in an mTORC1-dependent attenuation of L-lactate, the end product of glycolysis. Finally, we show that systemic administration of L-lactate attenuates mouse excessive alcohol intake. Our data suggest that alcohol promotes paradoxical actions of mTORC1 on translation and glycolysis which in turn drive excessive alcohol use.

Introduction

The mechanistic target of rapamycin (mTOR) is a ubiquitously expressed serine and threonine kinase that when localized with specific accessory proteins including the adaptor protein raptor, is termed mTORC1 (mTOR complex 1) (Liu and Sabatini, 2020). mTORC1 is activated by environmental cues such as amino acids, lipid, oxygen, nutrients such as glucose as well as through the activation of growth factor signaling (Liu and Sabatini, 2020; Napolitano et al., 2022). mTORC1 plays a central role in cell growth by promoting the translation of a subset of mRNAs to proteins, as well as well as by enhancing lipid and nucleotide signaling (Kim and Guan, 2019; Liu and Sabatini, 2020; Napolitano et al., 2022). In contrast, mTORC1 also contributes to catabolism through the suppression of lysosomal biogenesis autophagy (Napolitano et al., 2022) and to aging (Liu and Sabatini, 2020). mTORC1 also plays a crucial role in sensing and regulating feeding and fasting processes (Kim and Guan, 2019; Liu and Sabatini, 2020). In the central nervous system, mTORC1 is known for its actions to promote the translation of dendritic spine proteins (Lipton and Sahin, 2014; Santini et al., 2014). Specifically, upon activation mTORC1 phosphorylates its substrates the p70 ribosomal S6 kinase (S6K) and the eukaryotic translation initiation factor 4E binding protein (4E-BP). S6K then phosphorylates its substrate S6 (Costa-Mattioli et al., 2009), and these phosphorylation events promote the assembly of the translation initiation complex to initiate cap-dependent and independent mRNA translation of transcripts (Costa-Mattioli et al., 2009). mTORC1 together with its substrates are localized to ribosomes and the whole translation machinery is found in both cell body and dendrites (Costa-Mattioli et al., 2009). Not surprisingly, mTORC1 plays an important role in synaptic plasticity, learning and memory (Buffington et al., 2014; Lipton and Sahin, 2014; Stoica et al., 2011). Because of its important role in cellular homeostasis, dysregulation of mTORC1 functions results in pathologies such as cancer, obesity,

liver and pancreatic abnormalities (Liu and Sabatini, 2020) as well as neurodegenerative and neurodevelopmental diseases and psychiatric disorders (Costa-Mattioli and Monteggia, 2013; Lipton and Sahin, 2014) including addiction (Neasta et al., 2014).

Research on the mechanism(s) by which mTORC1 drives adverse phenotypes associated with drugs of abuse has not been explored much. We focused on the interaction between mTORC1 and alcohol and discovered that chronic excessive alcohol intake in rodents produces long-lasting activation of mTORC1 in discrete brain regions including the nucleus accumbens (NAc) (Barak et al., 2013; Laguesse et al., 2017a; Neasta et al., 2010). Using the selective mTORC1 inhibitor, rapamycin (Li et al., 2014), as well as its derivative, Rapalink-1 (Rodrik-Outmezguine et al., 2016), we discovered that mTORC1 participates in mechanisms underlying phenotypes such as excessive alcohol drinking, habitual alcohol seeking and relapse to alcohol use (Barak et al., 2013; Ben Hamida et al., 2019; Morisot et al., 2019; Neasta et al., 2010). To elucidate the mechanism(s) by which mTORC1 in the NAc drives excessive alcohol use, we conducted an RNAseq study and found that alcohol-mediated mTORC1 activation in the NAc of male mice led to the increase in the translation of 12 transcripts (Laguesse et al., 2017b). Among the identified transcripts was the postsynaptic protein, Prosapip1 (Laguesse et al., 2017b). We found that the translation of Prosapip1 is increased in response to alcohol-mediated mTORC1 activation, which in turn promoted the formation of F-Actin, leading to synaptic and structural plasticity, alcohol self-administration and reward (Laguesse et al., 2017b).

In addition, RNAseq data revealed that alcohol-dependent activation of mTORC1 in the NAc also led to increased translation of the microRNA machinery transcripts, Translin-associated factor X (Trax), GW182 (also known as Tnrc6a) and CCR4-NOT transcription complex subunit 4 (CNOT4) (Laguesse et al., 2017b). The microRNA machinery is responsible for the repression of

translation and mRNA degradation (Bartel, 2004; Gu and Kay, 2010). Here, we examined the potential crosstalk between alcohol, mTORC1 and microRNA function.

Results

Alcohol increases the translation of Trax and GW182 in an mTORC1-dependent manner in the NAc

As mentioned above, using RNAseq analysis we previously identified the microRNA machinery components Trax, GW182 and CNOT4 as candidate transcripts whose translation was increased by alcohol in an mTORC1-dependent manner (Laguesse et al., 2017b). To confirm the RNAseq data, male mice underwent intermittent access to 20% alcohol in a 2-bottle choice (IA20%2BC) paradigm for 7 weeks. This paradigm models humans who exhibit alcohol use disorder (AUD) (Carnicella et al., 2014). Three hours before the end of the last 24 hours alcohol withdrawal session, mice were systemically administered with vehicle or the selective mTORC1 inhibitor, rapamycin (20mg/kg). The NAc was removed 24 hours after the last alcohol withdrawal session, polysomes were purified to isolate actively translating mRNAs, and RT-qPCR analysis was conducted (**Figure 1A, Tables S1-2, alcohol drinking and statistical analysis)**. First, we replicated the published data (Laguesse et al., 2017b) in a new cohort of animals and confirmed that the translating levels of Trax were indeed increased by alcohol and reduced back to baseline when mice were first pretreated with the mTORC1 inhibitor, rapamycin (**Figure 1B**).We confirmed the RNAseq data and showed that the translation of GW182 is increased by alcohol in the NAc in an mTORC1-dependent manner (**Figure 1C**). In contrast, the RNAseq data of CNOT4 in total NAc were not replicated (**Figure 1D**).

Next, to determine whether alcohol increases Trax and GW182 transcription, a new cohort of mice underwent 7 weeks of IA20%2BC, the NAc was removed at the end of the last alcohol withdrawal session, and total mRNA levels were examined. We did not observe a change in the total amount of mRNA of either transcript (**Figure S1A-B, Tables S1-2)**. Together, these data suggest that alcohol increases the translation but not the transcription of the microRNA machinery components GW182 and Trax.

Finally, we analyzed the protein levels of Trax and GW182 in water and alcohol drinking mice and found that the levels of both proteins were increased in the NAc of mice consuming alcohol as compared to water only drinking mice (**Figure 1E-H, Tables S1-2**). This increase was specific to the NAc as the levels of Trax and GW182 were not altered by alcohol in a neighboring striatal region, the dorsolateral striatum (DLS) (**Figure S1C-F, Tables S1-2**). Together, these data suggest that chronic heavy alcohol use increases the levels of the microRNA machinery proteins Trax and GW182 in the NAc of drinking mice (**Figure 1I**).

Alcohol represses the translation of PPM1E, Aldolase A and Rbfox2 in an mTORC1-dependent manner in the NAc

The microRNA machinery is responsible for repression of translation or mRNA degradation (Bartel, 2004; Gu and Kay, 2010). We speculated that alcohol-mediated increase in the translation of Trax and GW182 may point towards an unexpected link between mTORC1 and the microRNA machinery. Interestingly, while analyzing the RNAseq data (Laguesse et al., 2017b), we observed that the translation of 32 transcripts was repressed by alcohol in an mTORC1-dependent manner (**Table S3**). We classified the transcripts and found that 37% of them belong to the signal transduction category, 31% are part of the DNA/RNA machinery, 12% transcripts are

associated with actin/cytoskeleton, and 12% with metabolic pathways **(Figure S2)**. We confirmed the RNAseq data of 3 random transcripts by measuring the mRNA levels in NAc polysomes of mice that underwent 7 weeks of IA20%2BC, and that were treated with vehicle or rapamycin (20 mg/kg) 3 hours before the last alcohol withdrawal session (**Figure 2A-C, Tables S1-2)**. We found that the translation of the glycolytic enzyme, Aldolase A (Penhoet et al., 1969) (**Figure 2A**), the serine/threonine Protein Phosphatase PPM1E (Mg2+/Mn2+ Dependent 1E) (Voss et al., 2011) (**Figure 2B**), and the RNA binding protein Rbfox2 (RNA binding fox 1 homolog 2) (Arya et al., 2014) (**Figure 2C**) was repressed by alcohol as compared to water only drinking mice. Importantly, we detected a reversal of translation repression in mice that were pre-treated with rapamycin (**Figure 2A-C**). In contrast, we did not observe a change in the total mRNA levels of the transcripts suggesting that alcohol decreases the translation but not the transcription of these 3 genes (**Figure S3A-C, Tables S1-2**).

Next, we analyzed the protein level of Aldolase A, PPM1E and Rbfox2 in water and alcohol drinking mice. We found that alcohol significantly decreases the level of the 3 proteins in the NAc (**Figure 2D-I, Tables S1-2**). The decrease was specific to the NAc, as the level of Aldolase A, PPM1E and Rbfox2 was not altered by alcohol in the DLS (**Figure S3D-I, Tables S1-2**). Together, these data suggest that chronic heavy alcohol drinking increases the levels of the microRNA machinery proteins Trax and GW182 in the NAc and concomitantly represses the translation of Aldolase A, PPM1E and Rbfox2 (**Figure 2J**).

Alcohol-mediated mTORC1-dependent increase and decrease in translation is localized to D1 NAc neurons

The NAc is composed mainly of two neuronal subpopulations, dopamine D1 receptor (D1) and dopamine D2 receptor (D2) expressing medium spiny neurons (MSN) (Gerfen and Surmeier, 2011). We previously found that mTORC1 is specifically activated in the shell but not the core of the NAc (Laguesse et al., 2017a). We further showed that the first drink of alcohol activates mTORC1 specifically in D1 neurons in the NAc shell (Beckley et al., 2016). First, to determine if heavy chronic alcohol use activates mTORC1 in D1 NAc MSN, male D1-Cre mice were crossed with RiboTag mice in which GFP-fused ribosomal subunit RPL10 is expressed in the presence of Cre recombinase, enabling the detection of D1 neurons (Lesiak and Neumaier, 2016) (**Figure 3A**). D1-Cre x RiboTag mice underwent 7 weeks of IA20%2BC and were sacrificed at the end of the last alcohol withdrawal session (**Figure 3B, Tables S1-2**). We found that alcohol significantly increased S6 phosphorylation in D1 neurons of the NAc shell (**Figure 3C-D**), and that only 8.9% of phosphoS6 positive neurons are not D1 neurons (**Figure 3E**). Together, these data suggest that the majority of mTORC1 activated by excessive alcohol use is localized to D1 NAc neurons.

Next, we examined whether mTORC1-dependent alterations in translation are also localized to D1 NAc MSNs. To do so, we utilized D1-Cre x RiboTag mice which contain a GFP tag for affinity purification of D1 neuron ribosomes allowing for the isolation of mRNAs actively undergoing translation in D1 MSNs (**Figure 3F**). D1-Cre x RiboTag mice underwent 7 weeks of IA20%2BC or water only, and mRNA levels were measured in the GFP immunoprecipitated fraction (**Figure 3F, Tables S1-2**). We detected an enrichment in Trax and GW182 translation in D1 NAc neurons (**Figure 3G-H**). Interestingly, we also detected an increase in the level of CNOT4 mRNA undergoing translation in D1 MSNs (**Figure 3I**). In parallel, translation of Aldolase A,

PPM1E, and Rbfox2 was attenuated by alcohol in NAc D1 MSNs (**Fig. 3j-L)**. Together, our data suggest that mTORC1-dependent translation activation and translation repression occur in NAc D1 neurons (**Figure 3M**).

Identification of microRNAs targeting PPM1E, Aldolase A and Rbfox2

To determine whether miRs are responsible for the translation repression of PPM1E, Aldolase A and Rbfox2, we performed *in silico* analyses using algorithmic prediction tools miRwalk, miRDB and TargetScan to identify putative microRNAs targeting the 3 repressed transcripts. miR15b-5p, miR25-3p, miR34a-5p and miR92a-3p were identified by all 3 prediction tools as potential specific miRs for PPM1E, Aldolase A, and Rbfox2 (**Figure 4A**). Interestingly, we found that the level of all 4 miRs was elevated by alcohol in the NAc, however, the expression of miR 127-3p which was used as a control and miR34a-3p were not altered by alcohol (**Figure 4B, Tables S1-2**). The alcohol-mediated increase in miRs levels was specific to the NAc since the levels of these miRs were not altered by alcohol in the DLS (**Figure S4, Tables S1-2**). Together, these data suggest the expression of miRs that are predicted to target Aldolase A, PPM2E and RbFox2 are increased in the NAc of mice that drink alcohol.

miR34a-5p targets Aldolase A in the NAc

We next focused on Aldolase A and its predicted miR, miR34a-5p. First, we examined if the alcohol-mediated increase in the expression of miR34a-5p in the NAc depends on mTORC1 and found that alcohol-mediated increase in miR34a-5p expression is attenuated in mice that were pretreated with rapamycin (**Figure 4C**, **Tables S1-2**). In contrast, the level of miR127-3p was unaltered in mice drinking alcohol and treated with rapamycin (**Figure 4D**, **Tables S1-2**). We

hypothesized that miR34a-5p is required for the repression of Aldolase A translation and speculated that miR34a-5p binds 3'UTR of Aldolase A. To test this possibility, we constructed luciferase expression plasmids containing Aldolase A 3'-UTR sequence or a mutant of the 3'UTR which does not contain the putative miR34a-5p interaction site (**Figure 5A-B**). Co-transfection of the miR34a-5p with Aldolase A 3'-UTR plasmids into HEK293 cells significantly suppressed luciferase activity, while co-transfection of Aldolase A 3'-UTR with a control miR did not affect the luciferase activity (**Figure 5C, Table S2**). Mutation of the miR binding site within the Aldolase A 3'-UTR sequence abolished the effect of miR34a-5p on the luciferase activity (**Figure 5C, Table S2**). These data demonstrate that Aldolase A 3'-UTR directly interacts with miR34a-5p. To test whether miR34a-5p is targeting Aldolase A *in vivo*, the NAc shell of mice was infected with a lentivirus expressing miR34a (Ltv-miR34a) (**Figure 5D**). As shown in **Figure 5E-F (Table S2)**, Aldolase A levels in the NAc were significantly reduced by miR34a overexpression. Together, these data suggest that miR34a is increased by alcohol via mTORC1 which in turn targets Aldolase A for translation repression.

Alcohol reduces glycolysis in the NAc via mTORC1

Aldolase A belongs to the family of the Fructose Diphosphate Aldolase enzymes (Penhoet et al., 1969). Aldolase A is highly expressed in neurons, and is the major isoform expressed in the striatum (Berardini et al., 1997; Wachsmuth et al., 1975). Aldolase C is also expressed in the brain (Thompson et al., 1982). We found that Aldolase C protein levels in the NAc were unaltered by alcohol (**Figure S5**). Aldolase A is a critical enzyme in glycolysis, a ten-step metabolic pathway resulting in the production lactate (Magistretti and Allaman, 2018), and of ATP molecules through the tricarboxylic acid (TCA) cycle in the mitochondria (Dienel, 2019). Aldolase A catalyzes the

conversion of Fructose 1,6-Bisphosphate (F1,6BP) to Glyceraldehyde 3-phosphate (G3P) and dihydroxyacetone phosphate (DHAP) (Dienel, 2019) (**Figure 6A**). Since alcohol represses Aldolase A translation and protein levels in the NAc, we hypothesized that alcohol-mediated activation of mTORC1 leads to a reduction in glycolysis. To examine the possibility, we first conducted a metabolomics study in which we used mice that underwent IA20%2BC for 7 weeks (**Tables S1**). Twenty-four hours after the last drinking session, the NAc was dissected followed by metabolites extraction and mass spectrometry analysis. We found that the end product of glycolysis, lactate (Magistretti and Allaman, 2018), as well as other metabolites within the TCA cycle such as citrate, a-ketoglutarate and malate, were reduced by alcohol (**Figure 6B, Table S2**), suggesting that alcohol reduces glycolysis in the NAc. The attenuation of glycolysis was also not due to changes in the expression of the main neuronal and astrocyte glucose or lactate transporters (**Figure S6**) (Laguesse et al., 2017b). Ter Horst reported that D1 MSNs in the NAc of mice regulate glucose tolerance sensitivity in the periphery (Ter Horst et al., 2018). We therefore investigated whether glucose tolerance was affected in alcohol drinking mice. As shown in **Figure S7**, blood glucose level during the glucose tolerance test was not altered by 4 or 7 weeks of IA20%2BC, suggesting that alcohol's effect on glucose metabolism is centrally localized.

To examine if alcohol-mediated reduction in lactate content is mTORC1-dependent, mice underwent 7 weeks of IA20%2BC (**Tables S1)**. Three hours before the end of the last withdrawal session, mice were treated with vehicle or rapamycin. We found that lactate content was significantly decreased by alcohol in mice pretreated with vehicle (**Figure 6C, Table S2**). In contrast, lactate content was back to basal levels in mice that consumed alcohol and that were pretreated with rapamycin (**Figure 6C, Table S2**). Together, these data suggest that a consequence

of the mTORC1↑/miR34a-5p↑/Aldolase A↓ pathway is the attenuation of glycolysis and the reduction in lactate content in the NAc (**Figure 6D**).

Overexpression of miR34a-5p increases whereas administration of L-Lactate reduces alcohol consumption

We previously found that mTORC1 in the NAc plays an important role in mechanisms underlying alcohol drinking behaviors (Laguesse et al., 2017b; Liu et al., 2017; Neasta et al., 2010). We therefore tested the possibility that the mTORC1↑/miR34a-5p↑/Aldolase A↓/Glycolysis↓Lactate↓ pathway in the NAc (**Figure 6D**) plays a role in alcohol consumption. We reasoned that if this pathway contributes to neuroadaptations that drive alcohol intake, then overexpression of miR34a-5p in the NAc which represses the translation of Aldolase A, will accelerate, whereas L-lactate supplement, will attenuate alcohol consumption. To test these possibilities, first the NAc shell of mice was infected with Ltv-miR34a or a Ltv-control virus that only contains the GFP sequence. Three weeks later, mice were subjected to IA20%2BC. As predicted, miR-34a overexpression accelerated alcohol drinking as compared to mice infected with Ltv-GFP (**Figure 7A, Table S2)**.

Next, a new cohort of mice underwent 7 weeks of IA20%2BC (**Table S1**) and was then treated with L-lactate (2g/kg) subcutaneously 30 minutes before a drinking session, and alcohol and water intake were measured. We found that systemic administration of L-lactate was sufficient to reduce binge alcohol intake (**Figure 7B, Table S2**). Attenuation of alcohol intake was not due to changes in mice locomotive activity (**Figure S8**). Alcohol and water intake at the end of the 24-hour drinking session was not affected by L-lactate (**Figure 7E-G**). Recently Lund et al. reported that the high amount of sodium in the L-lactate solution induces dehydration and significantly

increases water intake (Lund et al., 2023) (**Figure 7C-D, Table S2**). To rule out the possible effect of sodium on alcohol drinking, a solution of sodium chloride (NaCl iso-osmolar solution, 1g/kg) was administered 30 minutes before a drinking session, and alcohol and water intake was measured. NaCl-treated mice showed a significant increase in water consumption, whereas their alcohol intake was unchanged (**Figure S9, Table S2**). These results suggest that the decrease in alcohol consumption by L-lactate administration was driven by L-lactate and not by sodium.

We then assessed whether the L-lactate effect is specific to alcohol or is shared with other rewarding substances. A new cohort of mice underwent 2 weeks of IA 1% sucrose 2BC and was then treated with L-lactate (2g/kg) subcutaneously 30 minutes before a drinking session. We found that L-lactate administration did not alter sucrose intake (**Figure S10**). Together, our data imply that the signaling cascade that includes miR34a-5p and lactate drives alcohol intake (**Graphical abstract**).

Discussion

We found that alcohol by activating mTORC1 in the NAc increases the translation of microRNA machinery transcripts and the levels of miRs including miR34a-5p. Alcohol-dependent activation of mTORC1 also represses the translation of a number of transcripts including Aldolase A. We further showed that miR34a5p targets Aldolase A for translation repression. As a result of alcohol-mediated mTORC1-dependent reduction in Aldolase A levels in the NAc, glycolysis is inhibited, and lactate levels are reduced. We postulate that one of the consequences of the mTORC1↑/miR34a-5p↑/Aldolase A↓/glycolysis↓Lactate↓ pathway is the escalation of alcohol intake (**Graphical abstract**).

Justification of using only male mice in the study

Our studies focused on male mice as mTORC1 is not activated by alcohol in the NAc of female mice (Cozzoli et al., 2016; Ehinger et al., 2023). Interestingly whereas the basal level of phosphoS6 in the NAc male mice is low (Laguesse et al., 2017a), the basal level of phosphoS6 in females is variable (Ehinger et al., 2023). These data suggest a sex-specific interaction between alcohol and mTORC1 which is being investigated.

Heavy alcohol intake activates mTORC1 in the NAc to promote and repress translation

We previously showed that both binge alcohol drinking and withdrawal activate mTORC1 in the NAc (Laguesse et al., 2017a; Neasta et al., 2010). Here we show that mTORC1 activation as well as translation enhancement and repression by alcohol are localized to D1 neurons. What could be the mechanism for alcohol-mediated mTORC1 activation in the NAc? Withdrawal from alcohol drinking increases the glutamatergic tone in the brain (Hwa et al., 2017) and specifically in the NAc (Pati et al., 2016). Stimulation of glutamate metabotropic mGlu1/5 receptors activates mTORC1 in hippocampal neurons (Bockaert and Marin, 2015), and we previously found that stimulation of the NMDA receptor (NMDARs) activates mTORC1 in the orbitofrontal cortex (OFC) (Morisot et al., 2019). Thus, it is plausible that the release of glutamate by cortical inputs specifically onto D1-MSN triggers mTORC1 activation in NAc D1 MSNs and the initiation of the cascade. However, mTORC1 is also activated during binge drinking (Laguesse et al., 2017a; Neasta et al., 2010), a time point in which alcohol inhibits the NMDARs in the NAc (Wang et al., 2007). Interestingly, NMDAR inhibition activates mTORC1 in the prefrontal cortex (Li et al., 2010). Therefore, it is plausible that during binge drinking of alcohol, mTORC1 is activated by

NMDAR inhibition and that the activation is maintained via glutamate binding to the NMDAR and/or mGlu1/5 during withdrawal.

mTORC1 increases the translation of microRNA machinery transcripts in response to alcohol

RNAseq analysis aimed to identify alcohol-mediated mTORC1-dependent translatome suggested that alcohol enhances the translation of miR machinery proteins CNOT4, Trax and GW182 (Laguesse et al., 2017b). We found that Trax and GW182 translation was increased in the NAc and specifically in NAc shell D1 neurons of mice consuming alcohol. Interestingly, alcohol-mediated translation of CNOT4 was only detected in D1 neurons which could be due to CNOT4 signal being lost upon harvesting the whole NAc. Together, these data suggest that mTORC1 activation by alcohol upregulates the translation of Trax, GW182 and CNOT4 in D1 NAc shell neurons (**Figure 3M**). GW182 is an essential part of the translation repression machinery (Gebert and MacRae, 2019; Gu and Kay, 2010). Trax and its binding partner Translin were reported to promote mRNA degradation (Asada et al., 2014; Baraban et al., 2018). Chen et al. found that the mRNA silencing CCR4-NOT complex, which CNOT4 is part of, hooks onto GW182 and recruits DDX6 to repress miR-target mRNAs (Chen et al., 2014). Interestingly, in parallel to the increase in the translation of the microRNA machinery transcripts, we identified alcohol-mediated mTORC1-dependent translation repression as well as the elevation of levels of specific miRs (**Figs. 3M and 4E**). Further studies are required to test whether the increase in the translation of GW182, Trax and CNOT4 promotes as we predict the function and/or efficacy of the microRNA machinery.

Paradoxical role of mTORC1 in the repression of translation and the initiation of miR biosynthesis

Our RNAseq data suggest that one of the consequences of mTORC1 activation by alcohol in the NAc is the repression of translation of 32 transcripts. These data are unexpected as mTORC1's main role is to promote translation (Buffington et al., 2014; Santini et al., 2014), whereas miRs function is to degrade mRNAs and to repress translation (Bartel, 2004). Previous data suggest that miRs target components of mTORC1 signaling and thus inhibit mTORC1 function (Kar et al., 2021; Kye et al., 2014; Zhang et al., 2017). For instance, miR199a-3p and miR100 directly target mTOR itself (Kar et al., 2021; Kye et al., 2014), and activation of mTORC1 by high level of nutrients represses miRs biosynthesis by the mRNA degradation of Drosha (Zhang et al., 2017). Thus, the fact that mTORC1 activation under certain circumstances, e.g., heavy alcohol use promotes miRNA biosynthesis and represses the translation of numerous transcripts challenges the conventional notion and suggests context-specific effects of mTORC1 signaling on miR expression.

Interestingly, we observed that in parallel, alcohol increases the levels of miRs that were identified by bioinformatic tools to potentially target the 3 transcripts. Importantly, we show that alcohol-mediated biosynthesis of at least one of the miRs (miR34a-5p) depends on mTORC1, thus directly linking mTORC1 to the microRNA machinery. The miR34 family has been associated with neurodegenerative disease (Bazrgar et al., 2021), psychiatric disorders (Bazrgar et al., 2021; Dias et al., 2014; Haramati et al., 2011; Lai et al., 2016; Malmevik et al., 2016; McNeill et al., 2020; Murphy and Singewald, 2019) as well as fear, anxiety, stress (Bazrgar et al., 2021; Dias et al., 2014; Lai et al., 2016), memory deficits and cognition (Malmevik et al., 2016; McNeill et al., 2020). Here, we identified new roles for miR34a-5p that are localized to the NAc, e.g., repression

of Aldolase A translation and upregulation of alcohol drinking. Interestingly, Raab-Graham and colleagues previously reported that inhibition of rapamycin increased Kv1.1 synaptic levels in hippocampal dendrites (Raab-Graham et al., 2006) through miR129 (Sosanya et al., 2015; Sosanya et al., 2013), although in contrast to our study miR129 expression was mTORC1-independent (Sosanya et al., 2015; Sosanya et al., 2013).

Alcohol represses the translation of Aldolase A and reduces glycolysis in the NAc

We found that alcohol represses the translation of Aldolase A in the NAc. Aldolase A is an essential glycolytic enzyme that catalyzes the conversion of F1,6BP to G3P and DHAP (Pirovich et al., 2021). Glucose metabolism is the major source of fuel in the brain (Dienel, 2019). Through multiple steps, glucose is metabolized to pyruvate which is converted to acetyl-CoA to produce ATP through the TCA cycle (Dienel, 2019). Our data suggest that alcohol reduces glycolysis and the TCA cycle in the NAc. These data are in line with the findings by Volkow and colleagues that glucose metabolism in the brain is significantly decreased in subjects suffering from AUD (Tomasi et al., 2013; Volkow et al., 1992; Volkow et al., 2006; Volkow et al., 2015; Wang et al., 2003). In contrast to our results, mTORC1 was reported to increase glycolysis in skeletal muscle cells (Dutchak et al., 2018), macrophages (Kim et al., 2022), embryonic fibroblasts (Sun et al., 2011) and adipocytes (Xu et al., 2021). Our data showing that glycolysis is inhibited by alcohol via mTORC1, provide yet another unexpected role for mTORC1 and suggest again that mTORC1 function depends on context and/or cell type.

The NAc and other brain regions play a major role in neuroadaptations that underlie addiction (Xu et al., 2020) which are high energy consuming mechanisms that require ATP (Faria-Pereira and Morais, 2022). The finding that glycolysis is inhibited by alcohol bears the question

of what is the alternative energy source that is required for alcohol-dependent neuroadaptations in the NAc? Interestingly, mTORC1 was reported to increase the pentose phosphate pathway which could be an alternative energy source for neurons (Saxton and Sabatini, 2017). Another possibility is that Acetyl-CoA instead of being generated by pyruvate, is produced by medium-chain fatty acids (MCFAs) through fatty acid beta-oxidation (Panov et al., 2014). For instance, the medium-chain fatty acid octanoate can cross the blood brain barrier (Wlaz et al., 2015), and has been shown to directly contribute ~20% of energy in the rat brain (Ebert et al., 2003). Thus, it is possible that when glucose levels are low, acetyl-CoA is produced through fatty acid metabolism. Another potential mechanism relates to acetate being metabolized from alcohol in the liver and astrocytes (Jiang et al., 2013; Jin et al., 2021; Volkow et al., 2013). Acetate can be converted to acetyl-CoA which enters the TCA cycle. Thus, acetate may be an alternative energy source in the NAc.

Alcohol-mediated mTORC1 activation in the NAc decreases lactate levels

In addition to pyruvate being converted to acetyl-CoA, pyruvate is also the source of lactate the end product of glycolysis (Dienel and Hertz, 2001; Magistretti and Allaman, 2018). We found that withdrawal from excessive alcohol intake reduces lactate content in the NAc, a process that requires mTORC1. This finding suggests a vectorial signaling in which alcohol withdrawal activates mTORC1 which increases the biogenesis of miR34a-5p, in turn reducing the translation of Aldolase A leading to the attenuation of glycolysis and its final product, lactate (**graphical abstract**).

Lactate was initially thought to be produced solely by astrocytes and to be shuttled to neurons according to their energetic needs (Machler et al., 2016). However, the lactate shuttle model has been disputed in part due to discrepancies in stoichiometry and kinetics of lactate

production (Dienel, 2017). In fact, a large body of evidence have shown that glycolysis takes place in neurons (Cisternas et al., 2016; Diaz-Garcia et al., 2017; Dienel, 2019; Faria-Pereira and Morais, 2022; Gjedde and Marrett, 2001; Hollnagel et al., 2020; Li et al., 2023), and we recently showed that hippocampal neurons metabolize glucose which is required for their normal function (Li et al., 2023). As mTORC1 activation occurs essentially in D1 neurons and rapamycin administration effectively reverses the alcohol-mediated reduction in lactate levels, our model strongly suggests a specific reduction of lactate levels within D1 neurons.

For many years lactate was thought to be only a byproduct of glycolysis (Magistretti and Allaman, 2018). However, recent studies showed that lactate is a signaling molecule and a substrate for epigenetic modification (Dai et al., 2022; Hollnagel et al., 2020; Magistretti and Allaman, 2018). For example, secreted lactate is a ligand for the Gi-coupled hydroxycarboxylic acid receptor 1 (HCAR1) (de Castro Abrantes et al., 2019), and lactate binding to HCAR1 modulates neuronal network function and synaptic plasticity (de Castro Abrantes et al., 2019). In addition, lactate was shown to be a substrate for lactylation, a newly identified posttranslational modification on proteins including Histone H3 and Histone H1 resulting in enhanced gene transcription (Hagihara et al., 2021; Li et al., 2022; Zhang et al., 2019). Thus, it is plausible that alcohol-mediated reduction of lactylation is the reason for the large number of transcripts that are reduced by alcohol in the NAc.

Further studies reported that ketogenic diet which is given as a replacement for glucose reduces negative withdrawal symptoms in humans and mice (Bornebusch et al., 2021; Dencker et al., 2018; Wiers et al., 2021) and alcohol intake in rats (Wiers et al., 2021). Interestingly, ketogenic diet was shown to decrease mTORC1 activity in the hippocampus and the liver (McDaniel et al., 2011; Willemse et al., 2023). These data together with ours suggest an intriguing possibility that

like the hypodopaminergic state in AUD subjects which drives further drinking to alleviate allostasis symptoms, hypoglycolysis also promotes further drinking to supply the brain alternative energy source. Further investigation on this topic is warranted.

Finally, we show that subcutaneous administration of L-lactate significantly reduces alcohol consumption. Attenuation of lactate levels or its shuttling between astrocytes and neurons are associated with stress (Hagihara et al., 2021) and depression (Carrard et al., 2018; Cherix et al., 2022). Importantly, L-lactate administration reduces depressive-like symptoms in mice (Carrard et al., 2021), and we found that systemic administration of L-lactate in mice reduces alcohol but not sucrose intake. Together, these data and ours suggest that psychiatric disorders are associated with an imbalance in lactate levels in the brain and that adjusting lactate levels reduces adverse effects associated with alcohol and depression. Furthermore, these data provide preclinical data to suggest that L-lactate could be developed as a cost-effective readily available approach to treat AUD and potentially other psychiatric disorders.

In summary, this study unveils a novel dimension of mTORC1 function in alcohol-related behaviors. Specifically, our study unravels a paradoxical action of mTORC1 in orchestrating both translation repression and metabolic shift in response to chronic alcohol exposure which in turn drives further alcohol intake.

Methods

KEY RESOURCES TABLE

REAGENTS or RESOURCE	SOURCE	IDENTIFIER
Antibodies		
Rabbit anti-Aldolase A	Cell Signaling	3188s
Rabbit anti-PPM1E	Abnova	PAB21197
Rabbit anti-Rbfox2	Bethyl	A300-864A
Rabbit anti-Trax	Abgent	AP13947a
Rabbit anti-GW182	Sigma	SAB2102506-100UL
Mouse IgM anti-Tubulin	Santa Cruz Biotechnology	SC-8035
Mouse anti-GAPDH	Sigma	G8795
Rabbit anti-phospho S6 ribosomal protein	Cell Signaling	2211s
Chicken anti-GFP	Life Technologies	A10262
Guinea pig anti-NeuN	Millipore	ABN90
Donkey anti-rabbit horseradish peroxidase	Jackson ImmunoResearch	711-035-152
Donkey anti-mouse horseradish peroxidase	Jackson ImmunoResearch	715-035-150
Goat anti-mouse IgM horseradish peroxidase	Jackson ImmunoResearch	115-035-020
Donkey anti Rabbit Alexa fluor 488	Thermo Fisher Scientific	A21206
Goat anti Guinea Pig Alexa fluor 594	Thermo Fisher Scientific	A11076
Goat anti Chicken Alexa fluor 488	Thermo Fisher Scientific	A11039
Anti-GFP	Memorial Sloan-Kettering Monoclonal Antibody Facility	clone 19C8 and clone 19F7
Bacterial and Virus Strains		
Ltv-mir34a-5p	Generated in house	N/A
LentiLox 3.7 (pLL3.7) lentivirus	Addgene	11795
pLVX-IRES-GFP lentivirus	Clontech	632187

pmirGLO Dual-Luciferase miRNA Target Expression Vector	Promega	E1330
Critical Commercial Assays		
Ovation RNA-Seq	Tecan	System V2
miRCURY LNA RT kit	Qiagen	NA
miRCURY LNA RT kit	Qiagen	NA
miRCURY LNA SYBR Green master mix	Qiagen	NA
Qiagen Rneasy kit	Qiagen	NA
miRNeasy Mini Kit	Qiagen	NA
L-Lactate Assay Kit	Abcam	NA
Absolutely RNA Nanoprep kit	Agilent	NA
Plasmid Maxi Kit	Qiagen	NA
iScript cDNA Synthesis Kit	Biorad	
Oligonucleotides		
miR15b-5p	Qiagen	YP00204243
miR25-3p	Qiagen	YP00204361
miR34a-5p	Qiagen	YP00204486
miR92a-3p	Qiagen	YP00205947
miR127-3p	Qiagen	YP00204048
miR34a-3p	Qiagen	YP02108859
U6 snRNA	Qiagen	YP00203907
Trax	In house	F: GCTGGATGGTGTCAGACAGA; R: GAAAAGAGACAGCCTCCACG
GW182	In house	F: GCAGGGATTTAGTGCAAGAAG; R: GTGGAAGTGCCGTTATCAG
PPM1E	In house	F: GCCAGAGCCACATCAGATGA; R: AAGTCCTTCACCCAACTGCA
Aldolase A	In house	F: TAGCCGCGTTCGCTCCTTAG; R: CCTTCTTCTGCTCCGGGGTC
Rbfox2	In house	F: TCCGAGGAGACCATCTGAGG; R: AATCCGTCCTGGTAAACCACA
GAPDH	In house	F:

		CGACTTCAACAGCAACTCCCACTCTTCC; R: TGGGTGGTCCAGGGTTTCTTACTCCTT
mimic miR34a-5p	Invitrogen	4464066
mimic negative control	Invitrogen	4464058
Chemicals, Peptides, and Recombinant Proteins		
Nitrocellulose membranes	Millipore	NA
Enhance Chemiluminescence (ECL)	Millipore	NA
EDTA-free complete mini–Protease Inhibitor Cocktails	Roche	11873580001
Phosphatase inhibitor Cocktails 2 and 3	Sigma Aldrich	P5726 and P0044
Pierce bicinchoninic acid (BCA) protein assay kit	Thermo Scientific	23225
NuPAGE Bis-Tris precast gels	Life Technologies	NA
PowerUp SYBR Green master mix	Thermo Fisher Scientific	A25742
miRCURY LNA SYBR Green master mix	Qiagen	339345
Sodium L-Lactate	Sigma Aldrich	867-56-1
Rapamycin	LC Laboratories	R-5000
Ethyl alcohol	VWR	64-17-5
Cycloheximide	Sigma Aldrich	NA
1,2-diheptanoyl-sn-glycero-3-phosphocholine	Avanti Polar Lipids	NA
DL-DTT	Thermo Fisher Scientific	NA
HEPES, 1 M, pH 7.3, RNase-free	Affymetrix	NA
Magnesium chloride (MgCl2), 1 M, RNase-free	Thermo Fisher Scientific	NA
Methanol	Sigma Aldrich	NA

Nonylphenyl polyethylene glycol (NP-40)	Sigma Aldrich	NA
Rnasin Plus	Promega	NA
Streptavidin MyOne T1 Dynabeads	Thermo Fisher Scientific	NA
Biotinylated protein L	Thermo Fisher Scientific	NA
BSA, IgG and protease-free	Jackson ImmunoResearch	NA
Experimental Models: Cell Lines		
Neuro-2a	ATCC	CCL-131
Lenti-X 293T cells	Clontech	632180
Experimental Models: Mouse strains		
C57BL/6J	Jackson Laboratory	000664; RRID: IMSR_JAX:000664
Drd1a-Cre (D1-Cre)	Mutant Mice Resource and Research Centers (MMRRC) UC Davis (David, CA)	NA
AdoraA2-Cre (A2A-Cre)	MMRRC UC Davis (David, CA)	NA
ROSA26CAGGFP-L10a	Zhou et al., 2013	NA
Software and Algorithms		
ImageJ (NIH)	NIH	https://imagej.nih.gov/ij/
QuantStudio 5	Applied Biosystems	
TargetScan release 7.2	(Agarwal et al., 2015)	
miRWalk	(Sticht et al., 2018)	
miRDB	(Liu and Wang, 2019) (Chen and Wang, 2020)	

Resource availability

Lead contact

Further information and requests for resources and reagents should be directed to and will be fulfilled by the lead contact, Dorit Ron (dorit.ron@ucsf.edu).

Materials availability

Plasmids generated in this study and their sequences will be deposited to Addgene.

Experimental Models and Subject Details

Animals and Breeding

Male C57BL/6J mice (6-8 weeks old at time of purchase) were obtained from The Jackson Laboratory. Drd1a-Cre (D1-Cre) and AdoraA2-Cre (A2A-Cre) mice both of which are on C57BL/6 background, were obtained from Mutant Mice Resource and Research Centers (MMRRC) UC Davis. Ribotag mice (ROSA26CAGGFP-L10a), which express the ribosomal subunit RPL10a fused to EGFP (EGFP-L10a) in Cre-expressing cells (Zhou et al., 2013), were purchased from The Jackson Laboratory (B6;129S4-Gt (ROSA)26Sortm9(EGFP/Rpl10a)Amc/J). Ribotag mice were crossed with D1-Cre mice allowing EGFP-L10a expression in D1-expressing cells. Mouse genotype was determined by poly-chain reaction (PCR) analysis of tail DNA.

Only males (age 6-8 weeks) were used in the study. Mice were individually housed on paper-chip bedding (Teklad #7084), under a reverse 12-hour light-dark cycle (lights on 1000 to 2200 h). Temperature and humidity were kept constant at 22 ± 2°C, and relative humidity was maintained at 50 ± 5%. Mice were allowed access to food (Teklad Global Diet #2918) and tap water *ad libitum*. All animal procedures were approved by the university's Institutional Animal Care and Use Committee and were conducted in agreement with the Association for Assessment and Accreditation of Laboratory Animal Care.

Methods Details

Plasmids generation viral production

The mouse miR-34a nucleotide sequence (5'CCAGCTGTGAGTAATTCTTTGGCAGTGT CTTAGCTGGTTGTTGTGAGTATTAGCTAAGGAAGCAATCAGCAAGTATACTGCCCTA GAAGTGCTGCACATTGT3') was synthesized. Synthesized DNA oligos containing the miRNA sequences were annealed and inserted into pLL3.7 vector at HpaI and XhoI sites. Plasmids were prepared using a Plasmid Maxi Kit. All constructs were verified by sequencing.

The production of miR34a5p lentivirus was conducted as described in (Laguesse et al., 2017b). Briefly, HEK293 lentiX cells (Clontech, Mountain View, CA) were transfected with the lentiviral packaging vectors psPAX2 and pMD2.G, together with the pLL3.7 miR34a-5p or pLL3.7 GFP using lipofectamine 2000 in Opti-MEM medium. Six hours after transfection, medium was replaced to DMEM-FBS 10%. Sixty hours after transfection, supernatant containing the viral particles was collected, filtered into 0.22µm filters and purified by ultracentrifugation at 26.000 g for 90 minutes at 4°C. The pellet fraction containing the virus was resuspended in sterile PBS, aliquoted and stored at -80°C until use. Virus titer was determined using the HIV-1 p24 antigen ELISA kit.

Tissue harvesting

Mice were killed and brains were rapidly removed on an anodized aluminum block on ice. The NAc was isolated from a 1 mm thick coronal section located between +1.7 mm and +0.7 mm anterior to bregma according to the Franklin and Paxinos stereotaxic atlas (3rd edition). Collected tissues were immediately homogenized in 300 µl radioimmuno-precipitation assay (RIPA) buffer (50 mM Tris-HCl, pH 7.6, 150mM NaCl, 2mM EDTA, 1% NP-40, 0.1% SDS. and 0.5% sodium

deoxycholate and protease and phosphatase inhibitors cocktail). Samples were homogenized by a sonic dismembrator. Protein content was determined using a BCA kit.

Polysomal fractionation

Polysome-bound RNA was purified from mouse NAc according to a protocol we described previously (Liu et al., 2017). Specifically, fresh mouse NAc was snap-frozen in a 1.5ml Eppendorf tube and pulverized in liquid nitrogen with a pestle. After keeping on dry ice for 5 minutes, the powder of one NAc was resuspended in 1 ml lysis buffer (10mM Tris pH 8.0, 150mM NaCl, 5mM $MgCl_2$, 1% NP40, 0.5% sodium deoxycholate, 40mM dithiothreitol, 400U/ml Rnasin, 10mM Ribonucleoside Vanadyl Complex and 200µg/ml cycloheximide) followed by pipetting 20 times to further disrupt cell membranes. The homogenate was centrifuged for 10 seconds at 12.000g to remove intact nuclei. The supernatant was collected, and ribosomes were further released by adding 2X extraction buffer (200mM Tris pH7.5, 300mM NaCl and 200µg/ml cycloheximide). Samples were kept on ice for 5 minutes and then centrifuged at 12.000g, 4°C for 5 minutes to remove mitochondria and membranous debris. The resulting supernatant was loaded onto a 15%-45% sucrose gradient and centrifuged in a SW41Ti rotor at 38.000rpm, 4°C for 2 hours. Sucrose gradient fractions were collected and further digested with proteinase K solution (400µg/ml proteinase K, 10mM EDTA, 1% SDS) at 37°C for 30 minutes, followed by phenol-chloroform extraction. RNA in the water phase of the polysomal fraction was recovered by ethyl alcohol precipitation. The integrity of the polysomal fractions were confirmed as described in (Liu et al., 2017).

cDNA synthesis and real time quantitative PCR (RT-qPCR)

Total RNA extracted from tissues was treated with DNase I. Synthesis of cDNA was performed using the iScript cDNA Synthesis Kit according to the manufacturer's instructions. For polysomal RNA, and TRAP D1 RNA, cDNA synthesis and amplification were conducted using Ovation RNA Amplification Kit V2. The resulting cDNA was used for quantitative RT-qPCR, using SYBR Green PCR Master mix. Thermal cycling was performed on QuantStudio 5 real-time PCR System using a relative calibration curve. The quantity of each mRNA transcript was measured and expressed relative to Glyceraldehyde-3-Phosphate dehydrogenase (GAPDH). The Primers are listed in Key resources table.

***In Silico* miR prediction**

miRNA predictions were based on TargetScan 2 (Agarwal et al., 2015), miRwalk (Sticht et al., 2018) and miRDB (Chen and Wang, 2020; Liu and Wang, 2019). miR34a-5p and Aldolase A complimentary binding site was predicted using miRWalk (Sticht et al., 2018). miRWalk uses TarPmiR, a predictive algorithm, to generate a binding score (Sticht et al., 2018). Specifically, TarPmiR applies the trained random forest-based predictor to determine the target sites (Ding et al., 2016).

miRNA extraction, cDNA synthesis and quantitative RT-qPCR

microRNAs were extracted from tissues using miRNeasy Mini Kit according to the manufacturer's instructions. miRNAs yield and purity were evaluated using a nanodrop ND-1000 spectrophotometer. cDNA synthesis was performed using the miRCURY LNA RT kit according to the manufacturer's instructions, starting with 500ng of RNA and 5X reaction mix. Enzyme and

nuclease-free water was added to a final volume of 20µl. RNA spike-in of Unisp6 was added to each sample to monitor the efficiency of the reverse transcription reaction. Quantitative RT-qPCR was performed using miRCURY LNA SYBR Green master mix according to the manufacturer's instructions, and PCR samples were run on the QuantStudio 5. Each data point represents an average of 3 replicates. Relative microRNA expression was determined by the following calculation according to (Darcq et al., 2015). First, the average of cycle threshold (CT) of the miRNA of interest was subtracted from the CT of the control U6 rRNA to generate ΔCT. ΔCTs were then subtracted from the average of control ΔCT values for each sample to generate the ΔΔCT. miR levels were then calculated as 100 multiplied by $2^{-\Delta\Delta CT} \pm$ S.E.M. The Primers are listed in Key resources table.

TRAP purification

After NAc dissection, D1-specific mRNAs were purified according to the established TRAP protocol (Heiman et al., 2014). The NAc was homogenized with a glass homogenizer in an ice-cold lysis buffer (150mM KCl, 20mM HEPES [pH 7.4], 10mM MgCl2, 0.5mM dithiothreitol, 100µg/mL cycloheximide, 80U/µl RNasin Plus Rnase Inhibitor, and EDTA-free protease inhibitors). Following homogenization, samples were centrifuged at 2,000g at 4°C for 10 minutes and the supernatant was removed to a new tube. NP-40 (final concentration 1%) and 1,2-Diheptanoylsn-glycero-3-phosphocholine (DHPC, final concentration 15 mM) were subsequently added and samples were incubated on ice for 5 minutes. Samples were centrifuged at 20,000g at 4°C for 10 minutes and the supernatant was transferred to a new tube. Streptavidin Dynabeads coated with biotin-linked mouse anti-GFP antibodies were then added to the supernatant and the samples were incubated overnight at 4°C with end-over-end rotation. Beads were collected on a

magnetic rack and washed three times with wash buffer (350mM KCl, 20 mM HEPES pH 7.4, 10 mM $MgCl_2$, 0.5 mM dithiothreitol, 100µg/mL cycloheximide, 1% NP-40). RNA was subsequently purified using the Absolutely RNA Isolation Nanoprep kit. To ensure accurate quantitation, purified RNA was run on a Qubit 4.

Western blot analysis

Equal amounts of homogenates from individual mice (30µg) were resolved on NuPAGE Bis-Tris gels (4%-12% gradient) and transferred onto nitrocellulose membranes. Blots were blocked in 5% milk-PBS and 0.1% Tween 20 for 30 minutes and then incubated overnight at 4°C with primary antibodies. Membranes were then washed and incubated with HRP-conjugated secondary antibodies for 2 hours at room temperature. Bands were visualized using Enhanced Chemiluminescence (ECL). The optical density of the relevant band was quantified using ImageJ 1.44c software (NIH). Antibodies details are listed in Key resources table.

Immunochemistry

Mice were deeply anesthetized with Euthasol and perfused with 0.9% NaCl, followed by 4% paraformaldehyde in PBS, pH 7.4. Brains were removed, post-fixed in the same fixative for 2 hours, and transferred to PBS at 4°C. On the following day, brains were transferred into 30% sucrose and stored for 3 days at 4°C. Thirty µm-thick coronal sections were cut on a cryostat, collected serially and stored at -80°C. Sections were permeabilized with, and blocked in, PBS containing 0.3% Triton and 5% donkey serum for 4 hours. Sections were then incubated for 18 hours at 4°C on an orbital shaker with anti-pS6 (1:500) and anti-NeuN antibodies (1:500) diluted in 3% bovine serum albumin (BSA) in PBS. Next, sections were washed in PBS then incubated

for 4 hours with Alexa Fluor 596-labeled donkey anti-rabbit and Alexa Fluor 647-labeled donkey anti-mouse diluted in 3% BSA in PBS. After staining, sections were rinsed in PBS and cover slipped using Prolong Gold mounting medium. Images were acquired using an Olympus Fluoview 3000 Confocal microscope using manufacture recommended filter configurations. Quantification was preformed using the cell counter plugin in ImageJ software (NIH).

Luciferase assay

The 3′ untranslated region (UTR) of Aldolase A containing miR-34a-5p predicted target site was cloned into the pmirGLO Dual-Luciferase miRNA Target Expression Vector. Mutant construct was generated with a mutated target site. HEK293 cells were seeded in 96-well plates and co-transfected with luciferase reporters, miR-34a-5p, or a miR negative control. Firefly (FL) and Renilla (RL) luciferase activities were measured 48 hours after transfection using TECAN plate reader. Signal was calculated using FL/RL ratio relative to the empty pmirGLO reporter vector.

NAc shell viral infection

Intra-NAc shell infusion of lentivirus was conducted as described in (Laguesse et al., 2017b). Briefly, mice were anesthetized using isoflurane. Bilateral viral infusions were done using stainless steel injectors (33 gauge, Hamilton) into the NAc shell (anteroposterior +1.2 mm, mediolateral ± 0.75 mm and dorsoventral -4.30 mm, from bregma). Animals were infused with Ltv-Control expressing GFP only or Ltv-miR34a-5p (1.2×10^8 pg/ml, 1µl/side) at an infusion rate of 0.1µl/minute. After each infusion, the injectors were left in place for an additional 10 minutes to allow the virus to diffuse.

Preparation of solutions

Alcohol solution was prepared from absolute anhydrous alcohol (190 proof) diluted to 20% alcohol (v/v) in tap water.

rapamycin (20mg/kg) was dissolved in 5% DMSO and 95% saline. Vehicle contained 5% DMSO and 95% saline. Sodium L-Lactate (2g/kg) and NaCl (1g/kg) were dissolved in PBS as described in (Lund et al., 2023).

Drug administration

Rapamycin: rapamycin (20mg/kg) or vehicle were administered i.p. 3 hours before the end of the last alcohol withdrawal session and tissues were harvested at the end of the 24 hour withdrawal session as in (Laguesse et al., 2017b).

L-lactate: L-lactate (2g/kg) or NaCl (1g/kg) was administered subcutaneously (s.c.). A "within-subject" design in which mice received both treatments in counterbalanced order, with one week in between treatments. Specifically, on weeks 8 and 9, mice were administered s.c. with L-lactate (2g/kg), or vehicle solution 30 minutes before the beginning of the drinking session. On weeks 10 and 11, mice were systemically administered with NaCl (1g/kg), or vehicle 30 minutes before the beginning of the drinking session. Alcohol and water consumption was evaluated at the end of 4 hours and 24 hours drinking session.

Lactate measurement

The NAc lysates were added to 96-well plates and adjusted to 50µl of reaction mix as described in the lactate colorimetric assay kit instructions. After incubation for 30 minutes at room temperature in the dark, the absorbance at 570 nm was measured using a microplate reader.

Metabolomics

Metabolomics analysis was conducted as described in (Li et al., 2023). Specifically, fresh mouse NAc was snap-frozen in a 1.5ml Eppendorf tube in liquid nitrogen. To extract the metabolites from the frozen tissue, samples were first homogenized in a cryogenic mortar and pestle before being mixed with 1ml of 80% methanol chilled to −80°C. Samples were then vortexed for 20 seconds and incubated at -80°C for 20 minutes. Following the incubation, samples were vortexed for an additional 20 seconds and then centrifuged at 16,000g for 15 minutes at 4°C. The supernatant was transferred to a -80°C prechilled tube. BCA assay was used to normalize the extracted metabolites to protein content. A 100µg protein equivalent of extracted metabolites was aliquoted from each sample and dried in a CentriVap. The dried samples were then stored at -80°C until analysis by the UCLA Metabolomics Center.

Drinking paradigm

Two bottle choice - 20% alcohol

Mice underwent 7 weeks of intermittent access to 20% (v/v) alcohol in a two-bottle choice drinking paradigm (IA20%2BC) as previously described (Ehinger et al., 2021). Specifically, mice had 24-hour access to one bottle of 20% alcohol and one bottle of water on Mondays, Wednesdays, and Fridays, with alcohol drinking sessions starting 2 hours into the dark cycle. During the 24 or 48 hours (weekend) of alcohol withdrawal periods, mice had access to a bottle of water. The placement (right or left) of the bottles was alternated in each session to control for side preference. Two bottles containing water and alcohol in an empty cage were used to evaluate the spillage. Alcohol and water intake were measured at the end of each 24 hours drinking session (**Tables S1-2**).

Two bottle choice - 1% sucrose

Mice underwent 2 weeks of intermittent access to 1% (v/v) sucrose in a two-bottle choice drinking paradigm as previously described (Laguesse et al., 2017b). Specifically, mice had 24-hour access to one bottle of 1% sucrose and one bottle of water on Mondays, Wednesdays, and Fridays, with sucrose drinking sessions starting 2 hours into the dark cycle. The placement (right or left) of the bottles was alternated in each session to control for side preference. Two bottles containing water and sucrose in an empty cage were used to evaluate the spillage. Sucrose and water intake were measured at the end of each 24-hour drinking session.

Open field locomotion

Locomotion test was performed as described in (Warnault et al., 2016). Specifically, mice were habituated for 5 minutes in the open field apparatus (43 x 43 cm). Mice were then injected s.c. with 2g/kg L-lactate or saline before being placed back in the open field apparatus and their movement was recorded for an additional 20 minutes. Mice were automatically video tracked using Ethovision software and locomotion per 1-minute bins was calculated.

Glucose tolerance test

Glucose tolerance assay was performed as described previously (Ehinger et al., 2021). Briefly, mice were deprived of food for 6 hours and were then injected i.p. with 1 g/kg glucose. Blood samples were taken from a tail vein nick at different time intervals (0, 15, 30, 60, and 120 minutes post glucose administration), and blood glucose level was analyzed using a Bayer Contour blood glucose meter and test strips.

Statistical analysis

GraphPad Prism 7.0 (GraphPad Software Inc., La Jolla, CA) was used to plot and analyze the data. D'Agostino–Pearson normality and F-test/Levene tests were used to verify the normal distribution of variables and the homogeneity of variance, respectively. Data were analyzed using the appropriate statistical test, including two-tailed paired t-test, two-tailed unpaired t-test, one-way analysis of variance (ANOVA), and two-way ANOVA followed by post hoc tests as detailed in **Table S2**. All data are expressed as mean ± SEM, and statistical significance was set at $p < 0.05$.

Acknowledgments

This study was supported by the National Institute of Alcohol Abuse and Alcoholism, R01 AA027474 (D.R.), RF1 AG064170 and R01 AG065428 (K.N.) and F32 AG082460 (Y.J.S.). We thank Chhavi Shukla (University of California, San Francisco) for technical assistance.

References

Agarwal, V., Bell, G.W., Nam, J.W., and Bartel, D.P. (2015). Predicting effective microRNA target sites in mammalian mRNAs. Elife *4*, e05005.

Arya, A.D., Wilson, D.I., Baralle, D., and Raponi, M. (2014). RBFOX2 protein domains and cellular activities. Biochem Soc Trans *42*, 1180-1183.

Asada, K., Canestrari, E., Fu, X., Li, Z., Makowski, E., Wu, Y.C., Mito, J.K., Kirsch, D.G., Baraban, J., and Paroo, Z. (2014). Rescuing dicer defects via inhibition of an anti-dicing nuclease. Cell Rep *9*, 1471-1481.

Baraban, J.M., Shah, A., and Fu, X. (2018). Multiple Pathways Mediate MicroRNA Degradation: Focus on the Translin/Trax RNase Complex. Adv Pharmacol *82*, 1-20.

Barak, S., Liu, F., Ben Hamida, S., Yowell, Q.V., Neasta, J., Kharazia, V., Janak, P.H., and Ron, D. (2013). Disruption of alcohol-related memories by mTORC1 inhibition prevents relapse. Nat Neurosci *16*, 1111-1117.

Bartel, D.P. (2004). MicroRNAs: genomics, biogenesis, mechanism, and function. Cell *116*, 281-297.

Bazrgar, M., Khodabakhsh, P., Prudencio, M., Mohagheghi, F., and Ahmadiani, A. (2021). The role of microRNA-34 family in Alzheimer's disease: A potential molecular link between neurodegeneration and metabolic disorders. Pharmacol Res *172*, 105805.

Beckley, J.T., Laguesse, S., Phamluong, K., Morisot, N., Wegner, S.A., and Ron, D. (2016). The First Alcohol Drink Triggers mTORC1-Dependent Synaptic Plasticity in Nucleus Accumbens Dopamine D1 Receptor Neurons. J Neurosci *36*, 701-713.

Ben Hamida, S., Laguesse, S., Morisot, N., Park, J.H., Phuamluong, K., Berger, A.L., Park, K.D., and Ron, D. (2019). Mammalian target of rapamycin complex 1 and its downstream effector collapsin response mediator protein-2 drive reinstatement of alcohol reward seeking. Addict Biol *24*, 908-920.

Berardini, T.Z., Drygas-Williams, M., Callard, G.V., and Tolan, D.R. (1997). Identification of neuronal isozyme specific residues by comparison of goldfish aldolase C to other aldolases. Comp Biochem Physiol A Physiol *117*, 471-476.

Bockaert, J., and Marin, P. (2015). mTOR in Brain Physiology and Pathologies. Physiol Rev *95*, 1157-1187.

Bornebusch, A.B., Mason, G.F., Tonetto, S., Damsgaard, J., Gjedde, A., Fink-Jensen, A., and Thomsen, M. (2021). Effects of ketogenic diet and ketone monoester supplement on acute alcohol withdrawal symptoms in male mice. Psychopharmacology (Berl) *238*, 833-844.

Buffington, S.A., Huang, W., and Costa-Mattioli, M. (2014). Translational control in synaptic plasticity and cognitive dysfunction. Annu Rev Neurosci *37*, 17-38.

Carnicella, S., Ron, D., and Barak, S. (2014). Intermittent ethanol access schedule in rats as a preclinical model of alcohol abuse. Alcohol *48*, 243-252.

Carrard, A., Casse, F., Carron, C., Burlet-Godinot, S., Toni, N., Magistretti, P.J., and Martin, J.L. (2021). Role of adult hippocampal neurogenesis in the antidepressant actions of lactate. Mol Psychiatry *26*, 6723-6735.

Carrard, A., Elsayed, M., Margineanu, M., Boury-Jamot, B., Fragniere, L., Meylan, E.M., Petit, J.M., Fiumelli, H., Magistretti, P.J., and Martin, J.L. (2018). Peripheral administration of lactate produces antidepressant-like effects. Mol Psychiatry *23*, 488.

Chen, Y., Boland, A., Kuzuoglu-Ozturk, D., Bawankar, P., Loh, B., Chang, C.T., Weichenrieder, O., and Izaurralde, E. (2014). A DDX6-CNOT1 complex and W-binding pockets in CNOT9 reveal direct links between miRNA target recognition and silencing. Mol Cell *54*, 737-750.

Chen, Y., and Wang, X. (2020). miRDB: an online database for prediction of functional microRNA targets. Nucleic Acids Res *48*, D127-D131.

Cherix, A., Poitry-Yamate, C., Lanz, B., Zanoletti, O., Grosse, J., Sandi, C., Gruetter, R., and Cardinaux, J.R. (2022). Deletion of Crtc1 leads to hippocampal neuroenergetic impairments associated with depressive-like behavior. Mol Psychiatry *27*, 4485–4501.

Cisternas, P., Salazar, P., Silva-Alvarez, C., Barros, L.F., and Inestrosa, N.C. (2016). Activation of Wnt Signaling in Cortical Neurons Enhances Glucose Utilization through Glycolysis. J Biol Chem *291*, 25950-25964.

Costa-Mattioli, M., and Monteggia, L.M. (2013). mTOR complexes in neurodevelopmental and neuropsychiatric disorders. Nat Neurosci *16*, 1537-1543.

Costa-Mattioli, M., Sossin, W.S., Klann, E., and Sonenberg, N. (2009). Translational control of long-lasting synaptic plasticity and memory. Neuron *61*, 10-26.

Cozzoli, D.K., Kaufman, M.N., Nipper, M.A., Hashimoto, J.G., Wiren, K.M., and Finn, D.A. (2016). Functional regulation of PI3K-associated signaling in the accumbens by binge alcohol drinking in male but not female mice. Neuropharmacology *105*, 164-174.

Dai, X., Lv, X., Thompson, E.W., and Ostrikov, K.K. (2022). Histone lactylation: epigenetic mark of glycolytic switch. Trends Genet *38*, 124-127.

Darcq, E., Warnault, V., Phamluong, K., Besserer, G.M., Liu, F., and Ron, D. (2015). MicroRNA-30a-5p in the prefrontal cortex controls the transition from moderate to excessive alcohol consumption. Mol Psychiatry *20*, 1261.

de Castro Abrantes, H., Briquet, M., Schmuziger, C., Restivo, L., Puyal, J., Rosenberg, N., Rocher, A.B., Offermanns, S., and Chatton, J.Y. (2019). The Lactate Receptor HCAR1 Modulates Neuronal Network Activity through the Activation of G(alpha) and G(betagamma) Subunits. J Neurosci *39*, 4422-4433.

Dencker, D., Molander, A., Thomsen, M., Schlumberger, C., Wortwein, G., Weikop, P., Benveniste, H., Volkow, N.D., and Fink-Jensen, A. (2018). Ketogenic Diet Suppresses Alcohol Withdrawal Syndrome in Rats. Alcohol Clin Exp Res *42*, 270-277.

Dias, B.G., Goodman, J.V., Ahluwalia, R., Easton, A.E., Andero, R., and Ressler, K.J. (2014). Amygdala-dependent fear memory consolidation via miR-34a and Notch signaling. Neuron *83*, 906-918.

Diaz-Garcia, C.M., Mongeon, R., Lahmann, C., Koveal, D., Zucker, H., and Yellen, G. (2017). Neuronal Stimulation Triggers Neuronal Glycolysis and Not Lactate Uptake. Cell Metab *26*, 361-374 e364.

Dienel, G.A. (2017). Lack of appropriate Stoichiometry: Strong evidence against an energetically importand astrocytes-neuron lactate shuttle in the brain. *Journal of Neuroscience Research*, 2103.

Dienel, G.A. (2019). Brain Glucose Metabolism: Integration of Energetics with Function. Physiol Rev *99*, 949-1045.

Dienel, G.A., and Hertz, L. (2001). Glucose and lactate metabolism during brain activation. J Neurosci Res *66*, 824-838.

Ding, J., Li, X., and Hu, H. (2016). TarPmiR: a new approach for microRNA target site prediction. Bioinformatics *32*, 2768-2775.

Dutchak, P.A., Estill-Terpack, S.J., Plec, A.A., Zhao, X., Yang, C., Chen, J., Ko, B., Deberardinis, R.J., Yu, Y., and Tu, B.P. (2018). Loss of a Negative Regulator of mTORC1 Induces Aerobic Glycolysis and Altered Fiber Composition in Skeletal Muscle. Cell Rep *23*, 1907-1914.

Ebert, D., Haller, R.G., and Walton, M.E. (2003). Energy Contribution of Octanoate to Intact Rat Brain Metabolism Measured by 13C Nuclear Magnetic Resonance Spectroscopy. The Journal of Neuroscience *23*, 5928-5935.

Ehinger, Y., Phamluong, K., and Ron, D. (2023). Sexual differences in the interaction between alcohol and mTORC1. bioRxiv, 2023.2010.2004.560781.

Ehinger, Y., Zhang, Z., Phamluong, K., Soneja, D., Shokat, K.M., and Ron, D. (2021). Brain-specific inhibition of mTORC1 eliminates side effects resulting from mTORC1 blockade in the periphery and reduces alcohol intake in mice. Nat Commun *12*, 4407.

Faria-Pereira, A., and Morais, V.A. (2022). Synapses: The Brain's Energy-Demanding Sites. Int J Mol Sci *23*.

Gebert, L.F.R., and MacRae, I.J. (2019). Regulation of microRNA function in animals. Nat Rev Mol Cell Biol *20*, 21-37.

Gerfen, C.R., and Surmeier, D.J. (2011). Modulation of striatal projection systems by dopamine. Annu Rev Neurosci *34*, 441-466.

Gjedde, A., and Marrett, S. (2001). Glycolysis in neurons, not astrocytes, delays oxidative metabolism of human visual cortex during sustained checkerboard stimulation in vivo. J Cereb Blood Flow Metab *21*, 1384-1392.

Gu, S., and Kay, M.A. (2010). How do miRNAs mediate translational repression? Silence *1*, 11.

Hagihara, H., Shoji, H., Otabi, H., Toyoda, A., Katoh, K., Namihira, M., and Miyakawa, T. (2021). Protein lactylation induced by neural excitation. Cell Rep *37*, 109820.

Haramati, S., Navon, I., Issler, O., Ezra-Nevo, G., Gil, S., Zwang, R., Hornstein, E., and Chen, A. (2011). MicroRNA as repressors of stress-induced anxiety: the case of amygdalar miR-34. J Neurosci *31*, 14191-14203.

Heiman, M., Kulicke, R., Fenster, R.J., Greengard, P., and Heintz, N. (2014). Cell type-specific mRNA purification by translating ribosome affinity purification (TRAP). Nat Protoc *9*, 1282-1291.

Hollnagel, J.O., Cesetti, T., Schneider, J., Vazetdinova, A., Valiullina-Rakhmatullina, F., Lewen, A., Rozov, A., and Kann, O. (2020). Lactate Attenuates Synaptic Transmission and Affects Brain Rhythms Featuring High Energy Expenditure. iScience *23*, 101316.

Hwa, L., Besheer, J., and Kash, T. (2017). Glutamate plasticity woven through the progression to alcohol use disorder: a multi-circuit perspective. F1000Res *6*, 298.

Jiang, L., Gulanski, B.I., De Feyter, H.M., Weinzimer, S.A., Pittman, B., Guidone, E., Koretski, J., Harman, S., Petrakis, I.L., Krystal, J.H.*, et al.* (2013). Increased brain uptake and oxidation of acetate in heavy drinkers. J Clin Invest *123*, 1605-1614.

Jin, S., Cao, Q., Yang, F., Zhu, H., Xu, S., Chen, Q., Wang, Z., Lin, Y., Cinar, R., Pawlosky, R.J.*, et al.* (2021). Brain ethanol metabolism by astrocytic ALDH2 drives the behavioural effects of ethanol intoxication. Nat Metab *3*, 337-351.

Kar, A.N., Lee, S.J., Sahoo, P.K., Thames, E., Yoo, S., Houle, J.D., and Twiss, J.L. (2021). MicroRNAs 21 and 199a-3p Regulate Axon Growth Potential through Modulation of Pten and mTor mRNAs. eNeuro *8*, 0155-0121.

Kim, B., Kim, H.Y., Yoon, B.R., Yeo, J., In Jung, J., Yu, K.S., Kim, H.C., Yoo, S.J., Park, J.K., Kang, S.W.*, et al.* (2022). Cytoplasmic zinc promotes IL-1beta production by monocytes and

macrophages through mTORC1-induced glycolysis in rheumatoid arthritis. Sci Signal *15*, eabi7400.
Kim, J., and Guan, K.L. (2019). mTOR as a central hub of nutrient signalling and cell growth. Nat Cell Biol *21*, 63-71.
Kye, M.J., Niederst, E.D., Wertz, M.H., Goncalves Ido, C., Akten, B., Dover, K.Z., Peters, M., Riessland, M., Neveu, P., Wirth, B.*, et al.* (2014). SMN regulates axonal local translation via miR-183/mTOR pathway. Hum Mol Genet *23*, 6318-6331.
Laguesse, S., Morisot, N., Phamluong, K., and Ron, D. (2017a). Region specific activation of the AKT and mTORC1 pathway in response to excessive alcohol intake in rodents. Addict Biol *22*, 1856-1869.
Laguesse, S., Morisot, N., Shin, J.H., Liu, F., Adrover, M.F., Sakhai, S.A., Lopez, M.F., Phamluong, K., Griffin, W.C., 3rd, Becker, H.C.*, et al.* (2017b). Prosapip1-Dependent Synaptic Adaptations in the Nucleus Accumbens Drive Alcohol Intake, Seeking, and Reward. Neuron *96*, 145-159 e148.
Lai, Y.W., Chu, S.Y., Wei, J.Y., Cheng, C.Y., Li, J.C., Chen, P.L., Chen, C.H., and Yu, H.H. (2016). Drosophila microRNA-34 Impairs Axon Pruning of Mushroom Body gamma Neurons by Downregulating the Expression of Ecdysone Receptor. Sci Rep *6*, 39141.
Lesiak, A.J., and Neumaier, J.F. (2016). RiboTag: Not Lost in Translation. Neuropsychopharmacology *41*, 374-376.
Li, H., Guglielmetti, C., Sei, Y.J., Zilberter, M., Le Page, L.M., Shields, L., Yang, J., Nguyen, K., Tiret, B., Gao, X.*, et al.* (2023). Neurons require glucose uptake and glycolysis in vivo. Cell Rep *42*, 112335.
Li, J., Kim, S.G., and Blenis, J. (2014). Rapamycin: one drug, many effects. Cell Metab *19*, 373-379.
Li, N., Lee, B., Liu, R.J., Banasr, M., Dwyer, J.M., Iwata, M., Li, X.Y., Aghajanian, G., and Duman, R.S. (2010). mTOR-dependent synapse formation underlies the rapid antidepressant effects of NMDA antagonists. Science *329*, 959-964.
Li, X., Yang, Y., Zhang, B., Lin, X., Fu, X., An, Y., Zou, Y., Wang, J.X., Wang, Z., and Yu, T. (2022). Lactate metabolism in human health and disease. Signal Transduct Target Ther *7*, 305.
Lipton, J.O., and Sahin, M. (2014). The neurology of mTOR. Neuron *84*, 275-291.
Liu, F., Laguesse, S., Legastelois, R., Morisot, N., Ben Hamida, S., and Ron, D. (2017). mTORC1-dependent translation of collapsin response mediator protein-2 drives neuroadaptations underlying excessive alcohol-drinking behaviors. Mol Psychiatry *22*, 89-101.
Liu, G.Y., and Sabatini, D.M. (2020). mTOR at the nexus of nutrition, growth, ageing and disease. Nat Rev Mol Cell Biol *21*, 183-203.
Liu, W., and Wang, X. (2019). Prediction of functional microRNA targets by integrative modeling of microRNA binding and target expression data. Genome Biol *20*, 18.
Lund, J., Breum, A.W., Gil, C., Falk, S., Sass, F., Isidor, M.S., Dmytriyeva, O., Ranea-Robles, P., Mathiesen, C.V., Basse, A.L.*, et al.* (2023). The anorectic and thermogenic effects of pharmacological lactate in male mice are confounded by treatment osmolarity and co-administered counterions. Nat Metab *5*, 677-698.
Machler, P., Wyss, M.T., Elsayed, M., Stobart, J., Gutierrez, R., von Faber-Castell, A., Kaelin, V., Zuend, M., San Martin, A., Romero-Gomez, I.*, et al.* (2016). In Vivo Evidence for a Lactate Gradient from Astrocytes to Neurons. Cell Metab *23*, 94-102.
Magistretti, P.J., and Allaman, I. (2018). Lactate in the brain: from metabolic end-product to signalling molecule. Nat Rev Neurosci *19*, 235-249.

Malmevik, J., Petri, R., Knauff, P., Brattas, P.L., Akerblom, M., and Jakobsson, J. (2016). Distinct cognitive effects and underlying transcriptome changes upon inhibition of individual miRNAs in hippocampal neurons. Sci Rep *6*, 19879.

McDaniel, S.S., Rensing, N.R., Thio, L.L., Yamada, K.A., and Wong, M. (2011). The ketogenic diet inhibits the mammalian target of rapamycin (mTOR) pathway. Epilepsia *52*, e7-11.

McNeill, E.M., Warinner, C., Alkins, S., Taylor, A., Heggeness, H., DeLuca, T.F., Fulga, T.A., Wall, D.P., Griffith, L.C., and Van Vactor, D. (2020). The conserved microRNA miR-34 regulates synaptogenesis via coordination of distinct mechanisms in presynaptic and postsynaptic cells. Nat Commun *11*, 1092.

Morisot, N., Phamluong, K., Ehinger, Y., Berger, A.L., Moffat, J.J., and Ron, D. (2019). mTORC1 in the orbitofrontal cortex promotes habitual alcohol seeking. Elife *8*, e51333.

Murphy, C.P., and Singewald, N. (2019). Role of MicroRNAs in Anxiety and Anxiety-Related Disorders. Curr Top Behav Neurosci *42*, 185-219.

Napolitano, G., Di Malta, C., and Ballabio, A. (2022). Non-canonical mTORC1 signaling at the lysosome. Trends Cell Biol *32*, 920-931.

Neasta, J., Barak, S., Hamida, S.B., and Ron, D. (2014). mTOR complex 1: a key player in neuroadaptations induced by drugs of abuse. J Neurochem *130*, 172-184.

Neasta, J., Ben Hamida, S., Yowell, Q., Carnicella, S., and Ron, D. (2010). Role for mammalian target of rapamycin complex 1 signaling in neuroadaptations underlying alcohol-related disorders. Proc Natl Acad Sci U S A *107*, 20093-20098.

Panov, A., Orynbayeva, Z., Vavilin, V., and Lyakhovich, V. (2014). Fatty acids in energy metabolism of the central nervous system. Biomed Res Int *2014*, 472459.

Pati, D., Kelly, K., Stennett, B., Frazier, C.J., and Knackstedt, L.A. (2016). Alcohol consumption increases basal extracellular glutamate in the nucleus accumbens core of Sprague-Dawley rats without increasing spontaneous glutamate release. Eur J Neurosci *44*, 1896-1905.

Penhoet, E.E., Kochman, M., and Rutter, W.J. (1969). Ioslation of fructose diphosphate aldolases A, B, and C. Biochemistry *8*, 4391-4395.

Pirovich, D.B., Da'dara, A.A., and Skelly, P.J. (2021). Multifunctional Fructose 1,6-Bisphosphate Aldolase as a Therapeutic Target. Front Mol Biosci *8*, 719678.

Raab-Graham, K.F., Haddick, P.C., Jan, Y.N., and Jan, L.Y. (2006). Activity- and mTOR-dependent suppression of Kv1.1 channel mRNA translation in dendrites. Science *314*, 144-148.

Rodrik-Outmezguine, V.S., Okaniwa, M., Yao, Z., Novotny, C.J., McWhirter, C., Banaji, A., Won, H., Wong, W., Berger, M., de Stanchina, E.*, et al.* (2016). Overcoming mTOR resistance mutations with a new-generation mTOR inhibitor. Nature *534*, 272-276.

Santini, E., Huynh, T.N., and Klann, E. (2014). Mechanisms of translation control underlying long-lasting synaptic plasticity and the consolidation of long-term memory. Prog Mol Biol Transl Sci *122*, 131-167.

Saxton, R.A., and Sabatini, D.M. (2017). mTOR Signaling in Growth, Metabolism, and Disease. Cell *168*, 960-976.

Sosanya, N.M., Brager, D.H., Wolfe, S., Niere, F., and Raab-Graham, K.F. (2015). Rapamycin reveals an mTOR-independent repression of Kv1.1 expression during epileptogenesis. Neurobiol Dis *73*, 96-105.

Sosanya, N.M., Huang, P.P., Cacheaux, L.P., Chen, C.J., Nguyen, K., Perrone-Bizzozero, N.I., and Raab-Graham, K.F. (2013). Degradation of high affinity HuD targets releases Kv1.1 mRNA from miR-129 repression by mTORC1. J Cell Biol *202*, 53-69.

Sticht, C., De La Torre, C., Parveen, A., and Gretz, N. (2018). miRWalk: An online resource for prediction of microRNA binding sites. PLoS One *13*, e0206239.
Stoica, L., Zhu, P.J., Huang, W., Zhou, H., Kozma, S.C., and Costa-Mattioli, M. (2011). Selective pharmacogenetic inhibition of mammalian target of Rapamycin complex I (mTORC1) blocks long-term synaptic plasticity and memory storage. Proc Natl Acad Sci U S A *108*, 3791-3796.
Sun, Q., Chen, X., Ma, J., Peng, H., Wang, F., Zha, X., Wang, Y., Jing, Y., Yang, H., Chen, R.*, et al.* (2011). Mammalian target of rapamycin up-regulation of pyruvate kinase isoenzyme type M2 is critical for aerobic glycolysis and tumor growth. Proc Natl Acad Sci U S A *108*, 4129-4134.
Ter Horst, K.W., Lammers, N.M., Trinko, R., Opland, D.M., Figee, M., Ackermans, M.T., Booij, J., van den Munckhof, P., Schuurman, P.R., Fliers, E.*, et al.* (2018). Striatal dopamine regulates systemic glucose metabolism in humans and mice. Sci Transl Med *10*, eaar3752.
Thompson, R.J., Kynoch, P.A., and Willson, V.J. (1982). Cellular localization of aldolase C subunits in human brain. Brain Res *232*, 489-493.
Tomasi, D., Wang, G.J., and Volkow, N.D. (2013). Energetic cost of brain functional connectivity. Proc Natl Acad Sci U S A *110*, 13642-13647.
Volkow, N.D., Hitzemann, R., Wang, G.J., Fowler, J.S., Burr, G., Pascani, K., Dewey, S.L., and Wolf, A.P. (1992). Decreased brain metabolism in neurologically intact healthy alcoholics. Am J Psychiatry *149*, 1016-1022.
Volkow, N.D., Kim, S.W., Wang, G.J., Alexoff, D., Logan, J., Muench, L., Shea, C., Telang, F., Fowler, J.S., Wong, C.*, et al.* (2013). Acute alcohol intoxication decreases glucose metabolism but increases acetate uptake in the human brain. Neuroimage *64*, 277-283.
Volkow, N.D., Wang, G.J., Franceschi, D., Fowler, J.S., Thanos, P.P., Maynard, L., Gatley, S.J., Wong, C., Veech, R.L., Kunos, G.*, et al.* (2006). Low doses of alcohol substantially decrease glucose metabolism in the human brain. Neuroimage *29*, 295-301.
Volkow, N.D., Wang, G.J., Shokri Kojori, E., Fowler, J.S., Benveniste, H., and Tomasi, D. (2015). Alcohol decreases baseline brain glucose metabolism more in heavy drinkers than controls but has no effect on stimulation-induced metabolic increases. J Neurosci *35*, 3248-3255.
Voss, M., Paterson, J., Kelsall, I.R., Martin-Granados, C., Hastie, C.J., Peggie, M.W., and Cohen, P.T. (2011). Ppm1E is an in cellulo AMP-activated protein kinase phosphatase. Cell Signal *23*, 114-124.
Wachsmuth, E.D., Thoner, M., and Pfleiderer, G. (1975). The cellular distribution of aldolase isozymes in rat kidney and brain determined in tissue sections by the immuno-histochemical method. Histochemistry *45*, 143-161.
Wang, G.J., Volkow, N.D., Fowler, J.S., Franceschi, D., Wong, C.T., Pappas, N.R., Netusil, N., Zhu, W., Felder, C., and Ma, Y. (2003). Alcohol intoxication induces greater reductions in brain metabolism in male than in female subjects. Alcohol Clin Exp Res *27*, 909-917.
Wang, J., Carnicella, S., Phamluong, K., Jeanblanc, J., Ronesi, J.A., Chaudhri, N., Janak, P.H., Lovinger, D.M., and Ron, D. (2007). Ethanol induces long-term facilitation of NR2B-NMDA receptor activity in the dorsal striatum: implications for alcohol drinking behavior. J Neurosci *27*, 3593-3602.
Warnault, V., Darcq, E., Morisot, N., Phamluong, K., Wilbrecht, L., Massa, S.M., Longo, F.M., and Ron, D. (2016). The BDNF Valine 68 to Methionine Polymorphism Increases Compulsive Alcohol Drinking in Mice That Is Reversed by Tropomyosin Receptor Kinase B Activation. Biol Psychiatry *79*, 463-473.

Wiers, C.E., Vendruscolo, L.F., van der Veen, J.W., Manza, P., Shokri-Kojori, E., Kroll, D.S., Feldman, D.E., McPherson, K.L., Biesecker, C.L., Zhang, R.*, et al.* (2021). Ketogenic diet reduces alcohol withdrawal symptoms in humans and alcohol intake in rodents. Sci Adv *7*, eabf6780.

Willemse, L., Terburgh, K., and Louw, R. (2023). A ketogenic diet alters mTOR activity, systemic metabolism and potentially prevents collagen degradation associated with chronic alcohol consumption in mice. Metabolomics *19*, 43.

Wlaz, P., Socala, K., Nieoczym, D., Zarnowski, T., Zarnowska, I., Czuczwar, S.J., and Gasior, M. (2015). Acute anticonvulsant effects of capric acid in seizure tests in mice. Prog Neuropsychopharmacol Biol Psychiatry *57*, 110-116.

Xu, L., Nan, J., and Lan, Y. (2020). The Nucleus Accumbens: A Common Target in the Comorbidity of Depression and Addiction. Front Neural Circuits *14*, 37.

Xu, Y., Shi, T., Cui, X., Yan, L., Wang, Q., Xu, X., Zhao, Q., Xu, X., Tang, Q.Q., Tang, H.*, et al.* (2021). Asparagine reinforces mTORC1 signaling to boost thermogenesis and glycolysis in adipose tissues. EMBO J *40*, e108069.

Zhang, D., Tang, Z., Huang, H., Zhou, G., Cui, C., Weng, Y., Liu, W., Kim, S., Lee, S., Perez-Neut, M.*, et al.* (2019). Metabolic regulation of gene expression by histone lactylation. Nature *574*, 575-580.

Zhang, Y., Huang, B., Wang, H.Y., Chang, A., and Zheng, X.F.S. (2017). Emerging Role of MicroRNAs in mTOR Signaling. Cell Mol Life Sci *74*, 2613-2625.

Zhou, P., Zhang, Y., Ma, Q., Gu, F., Day, D.S., He, A., Zhou, B., Li, J., Stevens, S.M., Romo, D.*, et al.* (2013). Interrogating translational efficiency and lineage-specific transcriptomes using ribosome affinity purification. Proc Natl Acad Sci U S A *110*, 15395-15400.

Figure legends

Graphical abstract

(**A**) Alcohol activates mTORC1 signaling in D1+ NAc neurons which in turn increases the translation of GW182, Trax and CNOT4 and represses the translation of Aldolase A, Rbfox2 and PPM1E. In parallel, alcohol increases the levels of miR15b-5p, miR25-3p, miR92-3p and miR34a-5p which are predicted to target Aldolase A, Rbfox2 and PPM1E.

(**B**) Alcohol activates mTORC1 signaling in the NAc which increases the level of miR34a-5p repressing the translation of Aldolase A and decreasing the level of L-lactate, promoting further drinking.

Figure 1 – Alcohol via mTORC1 increases the translation of Trax and GW182 but not CNOT4 in the NAc

(**A**) Mice underwent 7 weeks of IA20%-2BC (**Table S1**). Control animals had access to water bottles only. Three hours before the end of the last alcohol withdrawal period, mice were systemically injected with 20 mg/kg rapamycin or vehicle. The nucleus accumbens (NAc) was dissected from each of the four mouse groups (water+vehicle, water+rapamycin, alcohol+vehicle, alcohol+rapamycin) at the end of the last alcohol withdrawal period, were subjected to polysomal fractionation and RT-qPCR analysis.

(**B-D**) Polysomal RNA levels of Trax (**B**), GW182 (**C**) and CNOT4 (**D**) were measured by RT-qPCR. Data are presented as the average ratio of each transcript to GAPDH±SEM and expressed as % of water+vehicle. Statistical analyses are depicted in **Table S2**. *$p<0.05$, **$p<0.01$, ***$p<0.001$, ns: non-significant.

(E-H) Trax (**E,G**) and GW182 (**F,H**) protein levels were determined by western blot analysis. ImageJ was used for optical density quantification. Data are presented as the average ratio of Trax or GW182 to Tubulin±SEM and are expressed as % of water control. Statistical analyses are depicted in **Table S2**. ***p < 0.001.

(**I**) Alcohol activates mTORC1 signaling in the NAc which in turn increases the translation of GW182 and Trax.

Figure 2 Alcohol via mTORC1 represses the translation of Aldolase A, PPM1E and Rbfox2 in the NAc

Mice underwent 7 weeks of IA20%-2BC (**Table S1**) and were treated with 20mg/kg rapamycin as described above. (**A-C**) Polysomal mRNA levels of Aldolase A (**A**), PPM1E (**B**) and Rbfox2 (**C**). Data are presented as the average ratio of each transcript to GAPDH±SEM and expressed as the % of water+vehicle. Statistical analyses are depicted in **Table S2**. **p < 0.01, ***p < 0.001.

(**D-I**) Aldolase A (**D,G**), PPM1E (**E,H**) and Rbfox2 (**F,I**) protein levels were determined by western blot analysis. Data are presented as the average ratio of Aldolase A, PPM1E and Rbfox2 to Tubulin±SEM and are expressed as the % of water control. Statistical analyses are depicted in **Table S2**. *p<0.05, **p<0.01, ***p<0.001.

(**J**) Alcohol activates mTORC1 signaling in the NAc which in turn decreases the translation of Aldolase A, Rbfox2, PPM1E.

Figure 3 Alcohol activates mTORC1, increases the translation of Trax, GW182 and CNOT, and decreases the translation of Aldolase A, PPM1E, Rbfox2 in NAc D1+ neurons

(A) D1-Cre mice were crossed with RiboTag mice allowing the expression of RPL10-EGFP in D1-expressing neurons.

(**B**) Mice underwent 7 weeks of IA20%2BC (**Table S1**). Brains were dissected at the end of the last 24-hour withdrawal session as in **Figure 1A** and processed for IHC or biochemistry analysis.

(**C**) IHC analysis of phospho-S6 levels the NAc shell D1 neurons of drinking mice compared to water controls. Representative images of NAc at 20x magnification labeled with phospho-S6 in red, RPL10-GFP in green and NeuN in magenta. Bar scale 100µm.

(**D**) Phospho-S6 and D1 labeled neurons are expressed as % of water controls. Statistical analyses are depicted in **Table S2**. ***p<0.001.

(**E**) % of D1+ vs. D1- neurons labeled as phosphoS6 positive neurons.

(**F**) Affinity purification of ribosomes from D1+ neurons by using anti-GFP magnetic beads followed by RNA isolation and RT-qPCR.

(**G-L**) Polysomal mRNA levels in D1+ neurons of Trax (**G**), GW182 (**H**), CNOT4 (**I**), Aldolase A (**J**), PPM1E (**K**), Rbfox2 (**L**) after alcohol withdrawal were determined by RT-qPCR. Data are presented as the average ratio of a transcript to GAPDH±SEM and expressed as % of water control. Statistical analyses are depicted in **Table S2**. *p<0.05, **p<0.01, ***p<0.001, ns: non-significant.

(**M**) Alcohol activates mTORC1 signaling in D1+ NAc neurons which in turn increases the translation of GW182, Trax and CNOT4 and represses the translation of Aldolase A, Rbfox2 and PPM1E.

Figure 4 Identification of miR15b-5p, miR25-3p, miR92-3p and miR34a-5p which are increased by alcohol in the NAc; Activation of mTORC1 is required for alcohol-mediated increase of miR34a-5p expression

(A) Potential miRNA-target interaction between miR-15b-5p, miR-25-3p, miR-92a-3p and miR34a-5p the transcripts of interest: PPM1E, Aldolase A and Rbfox2. miRNA-target interactions were determined using miRWalk, TargetScan and miRDB.

(B) Mice underwent 7 weeks of IA20%2BC or water only (**Table S1**). Three hours before the end of the last 24 hours of alcohol withdrawal, the NAc was removed and the expression of miR15b-5p, miR25-3p, miR34a-5p and miR92-3p, as well as miR127-3p and miR34a-3p, were measured by RT-qPCR. Statistical analyses are depicted in **Table S2**. **p<0.01, ***p<0.001, ns: non-significant.

(C-D) Mice underwent 7 weeks of IA20%2BC or water only (**Table S1**). Three hours before the end of the last 24 hours of alcohol withdrawal, mice were injected with rapamycin (20mg/kg) (R) or vehicle (V). Alcohol (A), W (Water). The levels of miR34a-5p (**C**) and miR127-3p (**D**) were measured by RT-qPCR. Statistical analyses are depicted in **Table S2**. *p<0.05, ns: non-significant.

(**E**) Alcohol increases the levels of miR15b-5p, miR25-3p, miR92-3p and miR34a-5p which are predicted to target the 3 transcripts shown in Figure 3. Alcohol-mediated miR34a-5p increase depends on mTORC1.

Figure 5 miR34a-5p interacts with Aldolase A 3'UTR and represses Aldolase A levels in the NAc

(A) Predicted interaction sites (in red) of miR34a-5p sequence (top) and Aldolase A 3'UTR (middle). Mutated Aldolase 3'UTR is shown at the bottom.

(**B)** Map of Aldolase A 3'UTR or mutant 3'UTR cloned into a luciferase reporter vector.

(**C)** HEK293 cells were co-transfected with a reporter vector containing Aldolase A 3'UTR or mutant 3'UTR and miR34a-5p or a negative control. Bar graph depicts average ± SD expressed as Firefly luminescence normalized to Renilla luminescence and relative to a reference control. Statistical analyses are depicted in **Table S2**. Gray bars: Aldolase A or mutant Aldolase A. Hatched green bars: Aldolase A or mutant Aldolase A + miR34a5p. Dotted blue bars: Aldolase A or mutant Aldolase A + miR control. **p<0.01, ***p<0.001, ns: non-significant.

(**D**) Lenti-miR-34a-GFP infected NAc neurons. (**E-F**) miR-34a-5p or GFP was expressed in the NAc and Aldolase A protein level was evaluated by western blot analysis, quantified as a ratio of Aldolase A/GAPDH and depicted as % of Aldolase A levels in the NAc of GFP infected mice. Statistical analyses are depicted in **Table S2**. *p<0.05.

Figure 6 Alcohol decreases TCA cycle metabolites, including lactate which depends on mTORC1

(**A**) Aldolase A in the glycolysis pathway converts F1,6BP to G3P and DHAP. Lactate is the final product of glycolysis.

(**B**) After 7 weeks of IA20%2BC (**Table S1**) or water only, the NAc was dissected after 24 hours of alcohol withdrawal and metabolite levels were measured. Data are presented as relative amount of individual metabolites in water vs. alcohol. Statistical analyses are depicted in **Table S2**. *p<0.05, ns: non-significant. # metabolites that were not included in the panel.

(**C**) Mice underwent 7 weeks of IA20%2BC (**Table S1**) or water only. Three hours before the end of the last alcohol withdrawal period, mice were systemically injected with 20mg/kg rapamycin or

vehicle. The NAc was dissected after 3 hours, and lactate level was measured using a colorimetric assay. Statistical analyses are depicted in **Table S2**. **p<0.01, ***p<0.001, ns: non-significant. (**D**) Alcohol reduces TCA metabolites in the NAc and lactate which depends on mTORC1.

Figure 7 Overexpression of miR34a-5p in the NAc increases whereas s.c. administration of L-lactate attenuates alcohol consumption

(A) The Nac of mice was infected with Ltv-GFP or Ltv-miR34a-5p-GFP in the NAc. Three weeks later, mice underwent IA20%2BC, and alcohol consumption was measured daily for 6 session. Statistical analyses are depicted in **Table S2**. **p<0.01. (**B-G**) Mice underwent 7 weeks of IA20%2BC (**Table S1**) or water only. Mice received a single administration of L-lactate (s.c. 2g/kg) or PBS on weeks 8th and 9th 30 minutes before the beginning of the 24 hours alcohol drinking session in a counterbalanced manner. Alcohol and water were measured at the 4 hours (**B-D**) and 24 hours (**E-G**) time points. Statistical analyses are depicted in **Table S2**. **p<0.01, ***p<0.001, ns: non-significant.

Supplementary Figure Legends

Figure S1 Alcohol does not alter the transcription of Trax and GW182 in the NAc and the protein levels in the DLS After 7 weeks of IA20%2BC (**Table S1**), the NAc of mice was dissected at the end of the 24 hours alcohol withdrawal session. Control animals had access to water only. **(A-B)** GW182 and Trax mRNA level was determined by RT-qPCR in the total mRNA sample. Data are presented as the average ratio of GW182 or Trax to GAPDH±SEM and expressed as % of water control. Statistical analyses are depicted in **Table S2**. ns: non-significant.

(C-D) Trax and GW182 protein levels in the DLS. (**E-F**) Data are presented as the average ratio of GW182 or Trax to Tubulin±SEM and are expressed as % of water control. Statistical analyses are depicted in **Table S2**. ns: non-significant.

Figure S2 Functional characterization of RNAseq transcripts whose translation are decreased by alcohol in an mTORC1-dependent manner. Functional categories were determined by an up-to-date literature search of each of the transcripts highlighting the transcripts' known function. Some proteins have several functions and are therefore found in multiple functional categories.

Figure S3 Alcohol does not alter the transcription of Aldolase A, PPM1E, Rbfox2 in the NAc and the protein level in the DLS After 7 weeks of IA20%2BC (**Table S1**), the NAc of mice was dissected at the end of the 24 hours alcohol withdrawal session. Control animals had access to water only. **(A-C)** Total Aldolase A (**A**), PPM1E (**B**), Rbfox2 (**C**) mRNA levels were determined by RT-qPCR in the total mRNA sample. Data are presented as the average ratio of Aldolase A, Rbfox2 or PPM1E to GAPDH±SEM and expressed as % of water control. Statistical analyses are depicted in **Table S2**. ns: non-significance.

(D-F) Aldolase A, PPM1E, Rbfox2 protein levels after withdrawal were determined by western blot analysis. (**G-I**) Data are presented as the average ratio of Aldolase A, PPM1E, Rbfox2 to Tubulin±SEM and are expressed as the % of water control. Statistical analyses are depicted in **Table S2**. ns: non-significant.

Figure S4 The levels of miR15b-5p, miR25-3p, miR92a-3p, and miR34a-5p are not altered in the DLS After 7 weeks of IA20%2BC (**Table S1**), the NAc of mice was dissected at the end of the 24 hours alcohol withdrawal session. Control animals had access to water only. miRs levels were measured by RT-qPCR. Statistical analyses are depicted in **Table S2**. ns: non-significant.

Figure S5 Alcohol does not alter the protein levels of Aldolase C in the NAc

After 7 weeks of IA20%2BC (**Table S1**), the NAc of mice was dissected at the end of the 24 hours alcohol withdrawal session (A, red). Control animals had access to water only (W, white). **(A)** Aldolase C level was determined by western blot analysis. (**B**) Data are presented as the average ratio of Aldolase C to Tubulin±SEM and are expressed as % of water control. Statistical analyses are depicted in **Table S2**. ns: non-significant.

Figure S6 Alcohol does not alter the translation of the main glucose and lactate transporters in the NAc

After 7 weeks of IA20%2BC, the NAc of mice was dissected at the end of the 24 hours alcohol withdrawal session (A, red). Control animals had access to water only (W, white). RNAseq data (Laguesse et al., 2017b) revealed that the translation of the astrocytic glucose transporter Glu1 (**A**), the neuronal glucose transporter Glu3 (**B**), the neuronal lactate transporter MTC2 (**C**) and the astrocytic lactate transporter MTC4 **(D**) is unaltered by alcohol. W: water, A: alcohol, n=3. ns: non-significant. FPKM: Fragments per kilobase of transcript per million mapped reads

Figure S7 Blood glucose tolerance is unaltered by chronic alcohol drinking (**A-B**) Glucose tolerance test was performed after 4 weeks (**A**) and 7 weeks (**B**) of IA20%2BC (**Table S1**). Control

animals had access to water only. Mice were subjected to 6 hours fasting before glucose (1g/kg) injection. Blood was collected before glucose injection 15-120 minutes post glucose administration, and glucose levels were determined. Statistical analyses are depicted in **Table S2**.

Figure S8 L-lactate administration does not affect locomotion Mice were habituated for 5 minutes in the open field apparatus. Mice were then injected s.c. with 2g/kg L-lactate or PBS before being placed back in the open field and movement was recorded for an additional 20 minutes. Locomotion is depicted in 1-minute bins. Statistical analyses are depicted in **Table S2**. ns: non-significant.

Figure S9 Systemic administration of NaCl does not affect alcohol consumption

Mice underwent 7 weeks of IA20%2BC (**Table S1**) whereas control animals had access to water bottles only. On weeks 10 and 11, mice were s.c. injected with NaCl (1g/kg) or PBS in a counterbalanced manner 30 minutes before the beginning of a 24-hour drinking session. Alcohol and water consumption was measured at 4 hours (**A-C**) and 24 hours (**D-F**) timepoints. Statistical analyses are depicted in **Table S2**. *$p<0.05$, **$p<0.01$. ns: non-significant.

Figure S10 Systemic administration of L-lactate does not affect sucrose consumption

Mice underwent 2 weeks of IA1%Sucrose2BC. Control animals had access to water only. On weeks 3 and 4, mice were s.c. injected with L-lactate (2g/kg) or PBS in a counterbalanced manner 30 minutes before the beginning of a 24-hour drinking session. Sucrose and water intake were measured 4 hours (**A-C**) and 24 hours (**D-F**) later. Statistical analyses are depicted in **Table S2**. ns: nonsignificant.

Table S1 Alcohol drinking averages of mouse groups used in the study

Shown are average alcohol intake +/- SEM of the last 3 24 hours sessions for each of the experimental groups.

Table S2 Statistical analyses of the data

Shown are figure number, number of animals or replicates, statistical test and statistical analysis.

Table S3 Alcohol decreases the translation of transcripts in an mTORC1 dependent manner

After 7 weeks of IA20%2BC, the NAc of mice was dissected at the end of the 24 hours alcohol withdrawal session. Control animals had access to water only. RNAseq data (Laguesse et al., 2017b) are sorted in ascending order of fold change of alcohol+vehicle divided by water+vehicle with negative values indicating decreased translation by alcohol. Positive fold change of alcohol+vehicle divided by alcohol+rapamycin indicates a reversal of translation attenuation by rapamycin. Student-t-test n = 3.

Graphical Abstract

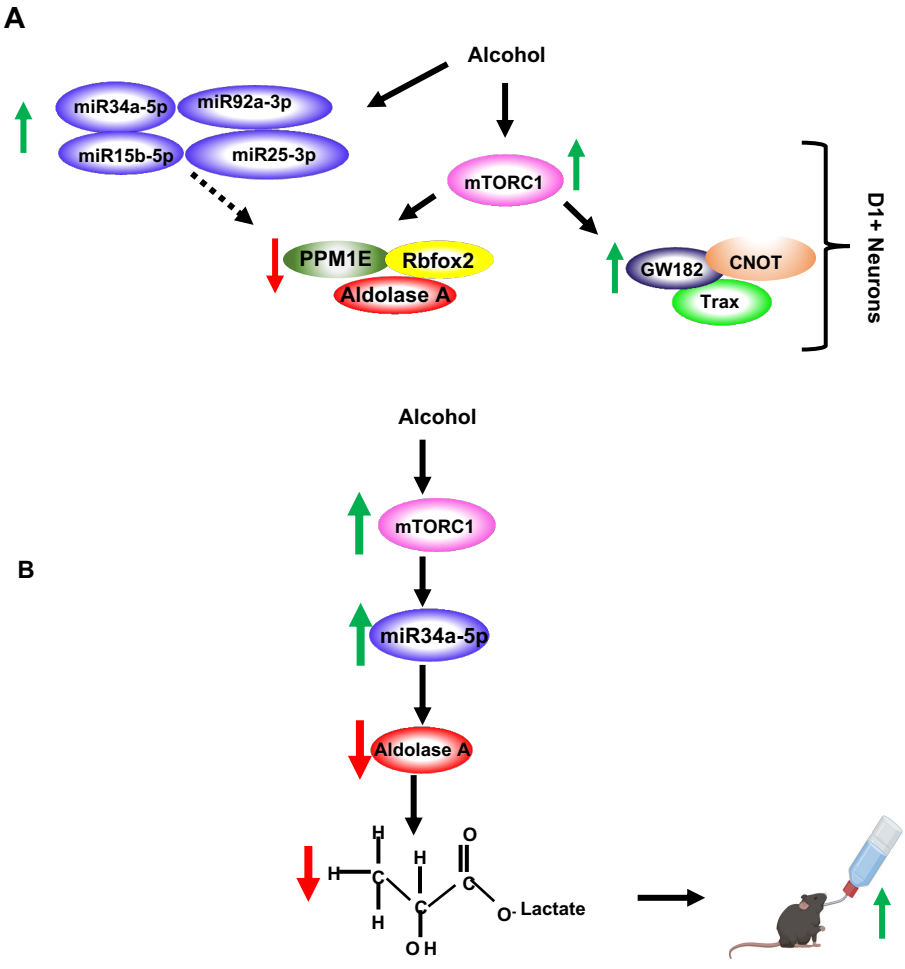

Figure 1: Alcohol via mTORC1 increases the translation of Trax and GW182 but not CNOT4 in the NAc

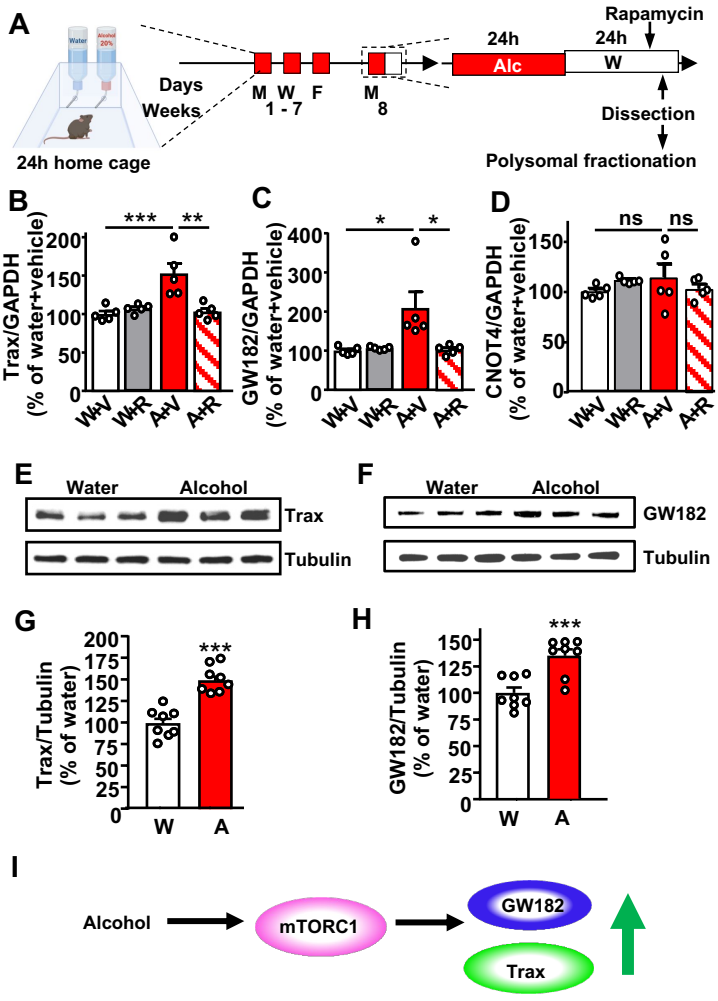

Figure 2: Alcohol via mTORC1 represses the translation of Aldolase A, PPM1E and Rbfox2 in the NAc

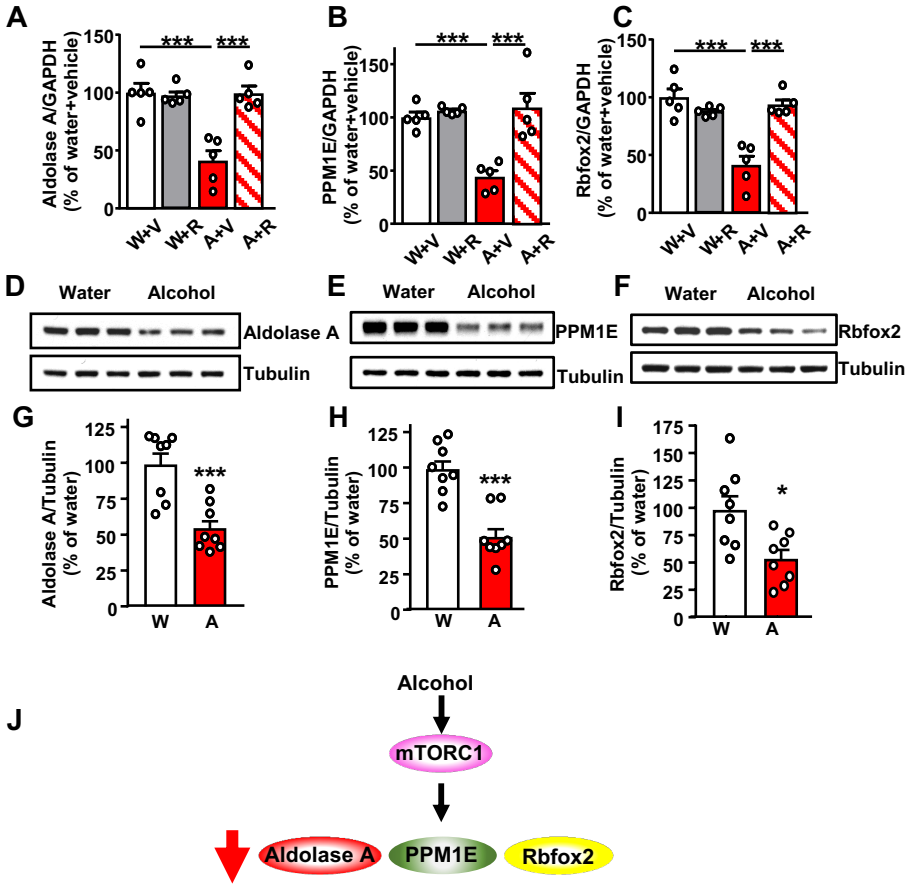

Figure 3: Alcohol activates mTORC1, increases the translation of Trax, Gw182 and CNOT4, and decreases the translation of Aldolase A, PPM1E and Rbfox2 D1+ neurons

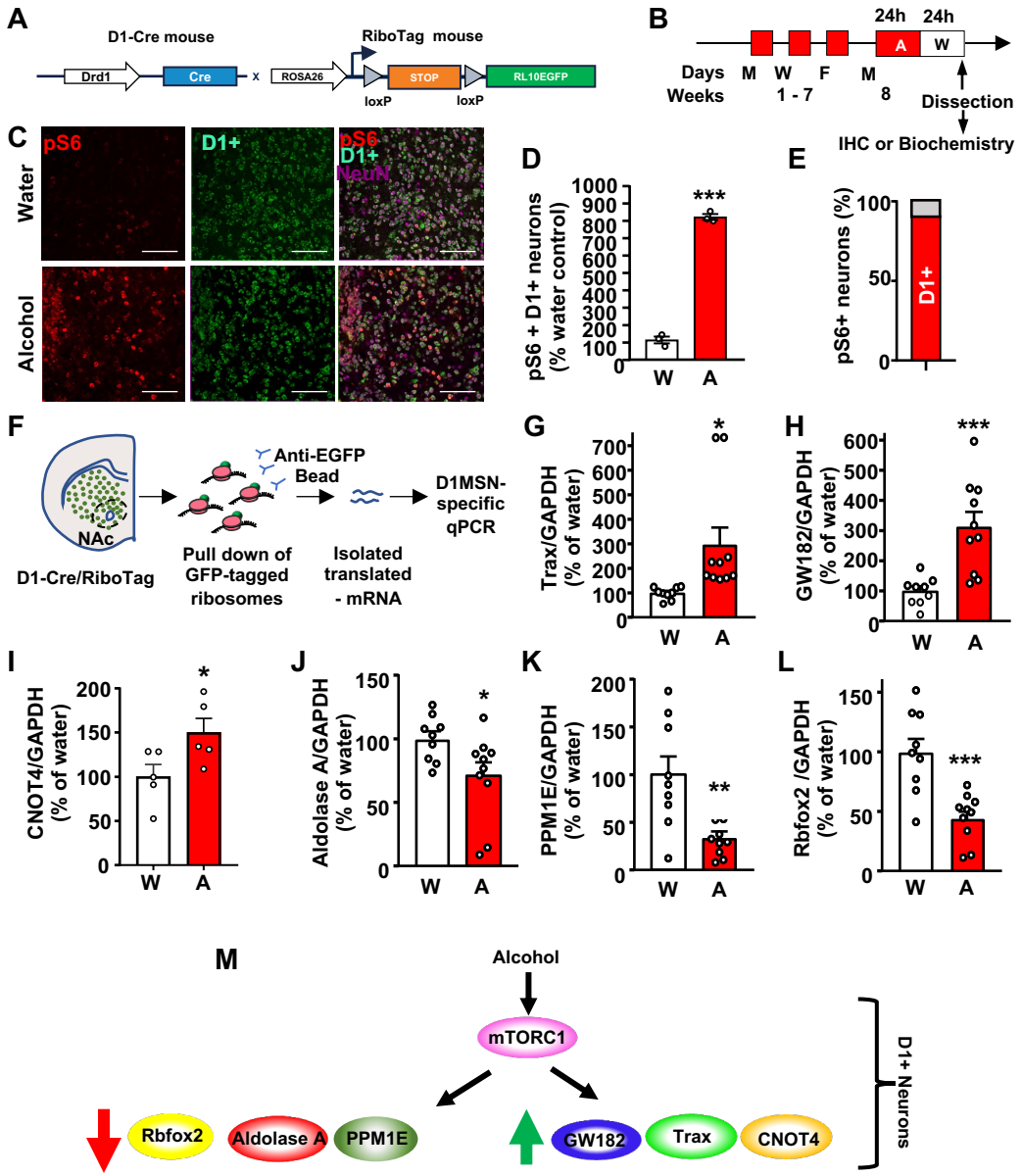

Figure 4 Identification of miR15b-5p, miR25-3p, miR34a-5p and miR92-3p which are increased in the NAc by alcohol; Activation of mTORC1 is required for alcohol-mediated increase of miR34a5p expression in the NAc

A

Gene Symbol	Refseq ID	miR15b-5p	miR25-3p	miR34a-5p	miR92a-3p	Prediction Tool
Aldoa	NM_001177307			y		miRwalk
				y		TargetScan
				y		miRDB
Rbfox2	NM_175387				y	miRwalk
			y		y	TargetScan
			y		y	miRDB
PPM1E	NM_177167	y	y	y	y	miRwalk
		y				TargetScan
		y	y		y	miRDB

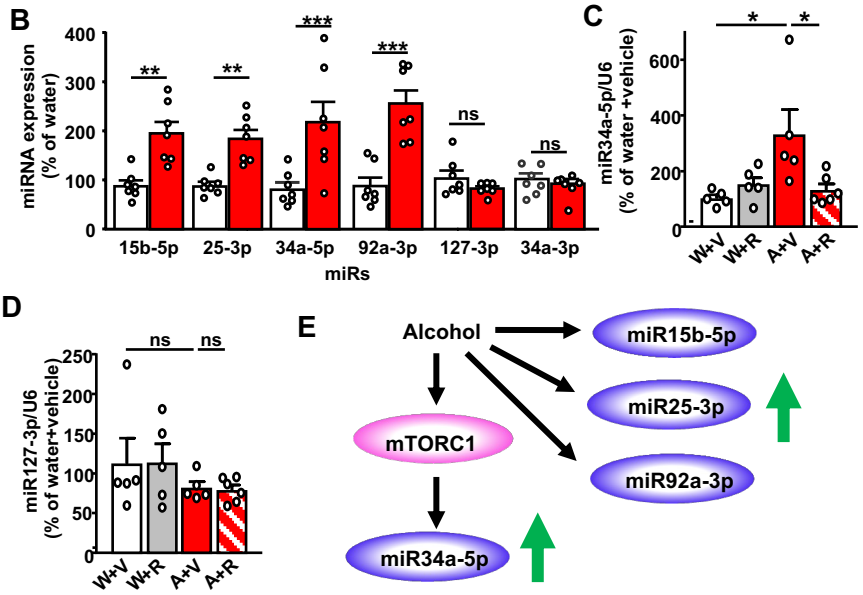

Figure 5: miR34a-5p interacts with Aldolase A 3'UTR and represses Aldolase A levels in the NAc

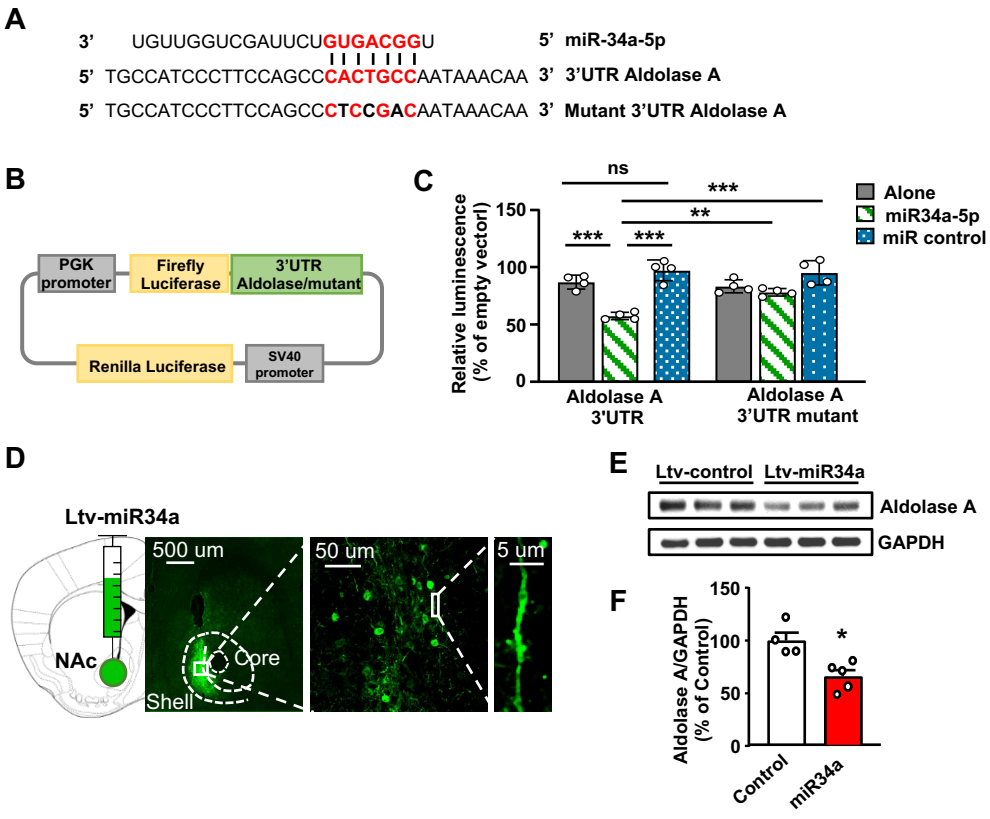

Figure 6: Alcohol decreases TCA cycle metabolites, including lactate which depends on mTORC1

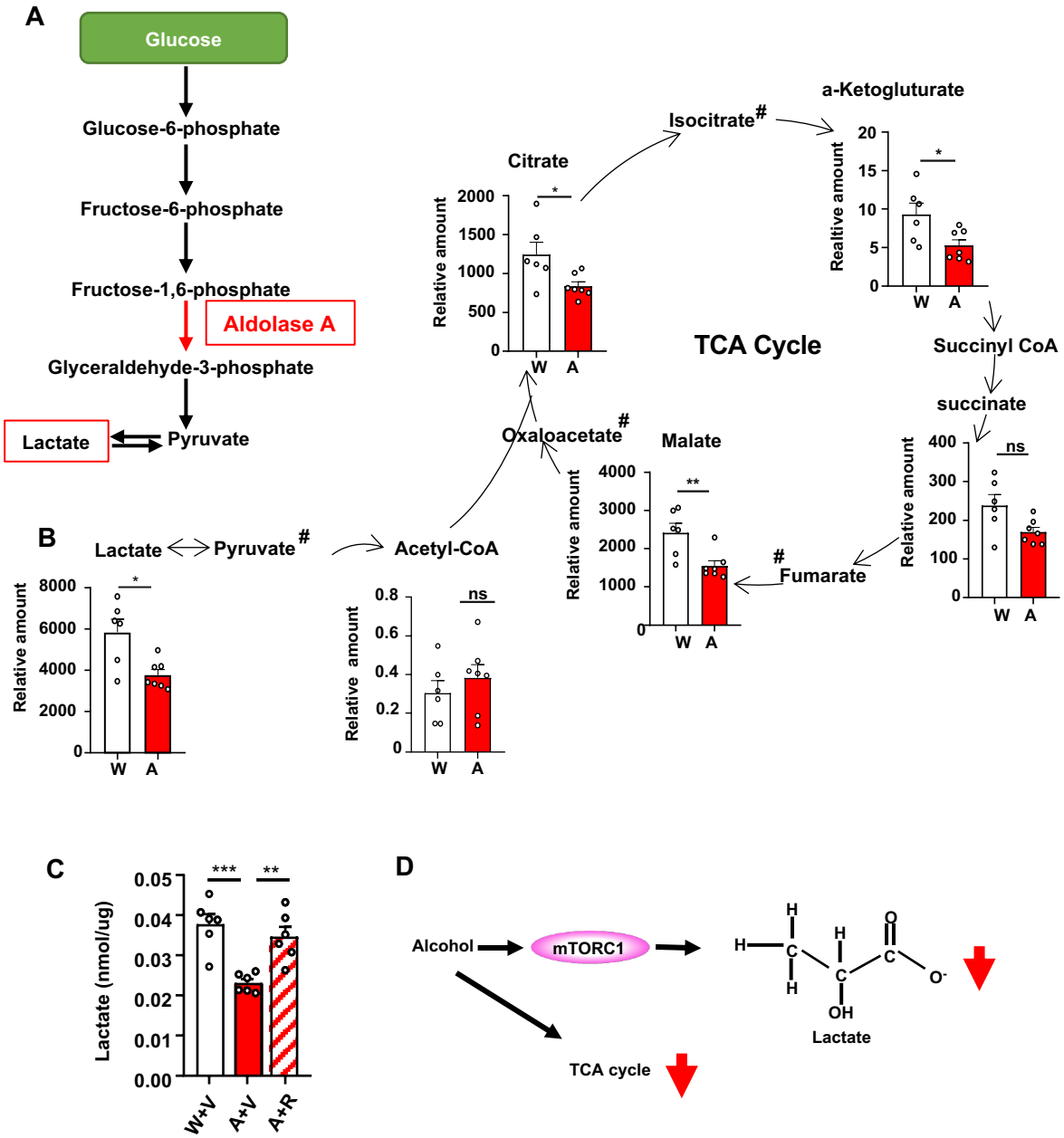

Figure 7: Overexpression of miR34a-5p in the NAc increases whereas s.c. administration of L-lactate attenuates alcohol consumption

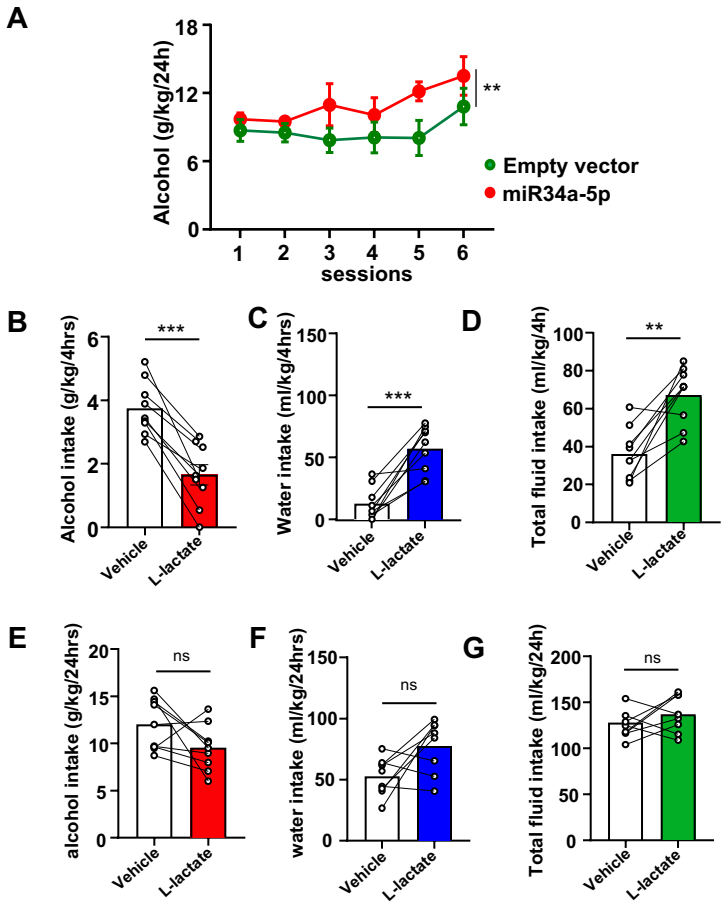

Figure S1: Alcohol does not alter the transcription of Trax and GW182 in the NAc and the protein levels of GW182 and Trax in the DLS

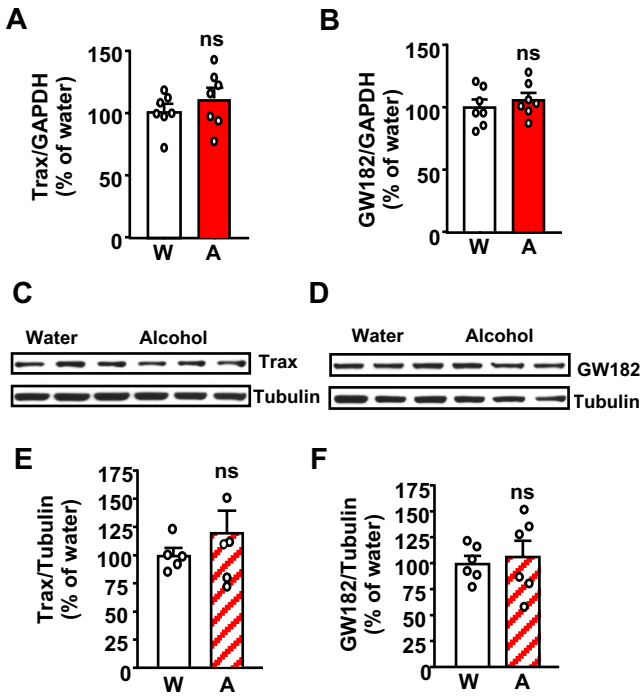

Figure S2: Categories of transcripts that are reduced by alcohol in an mTORC1 dependent manner

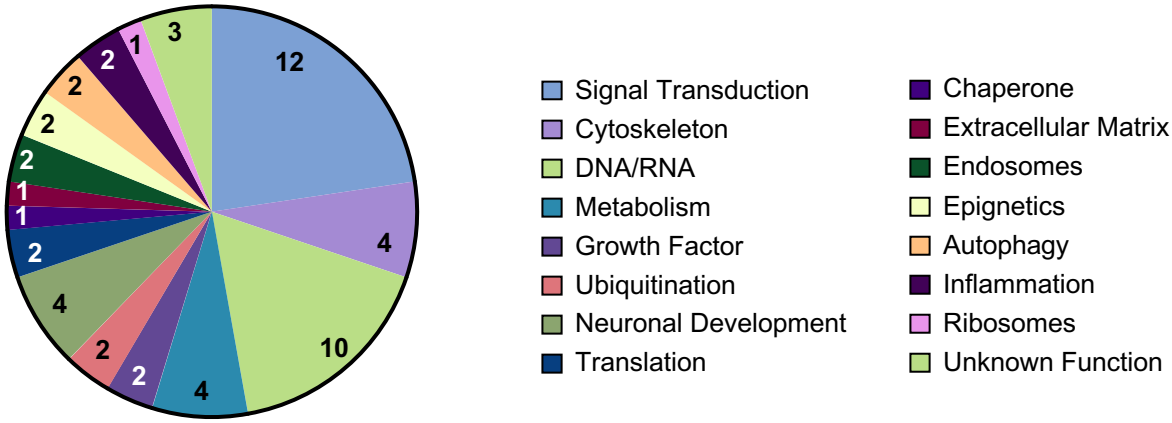

Signal Transduction
Klhl3 (Kelch-like 3)
Pdlim1(PDZ and Lim domain 1)
Ccdc93 (coiled-coil domain containing 93)
Flt1 (FMS-like tyrosine kinase 1)
PPM1E Protein phosphatase 1E
Pde4dip (phosphodiesterase 4D interacting protein)
Robo3 (Roundabout guidance receptor 3)
Tsc1 (tuberous sclerosis 1)
Igtp (Interferon gamma induced GTPase)
Dennd3 (DENN Domain Containing 3)
RIOK2 (RIO Kinase 2)
bHlha9 (basic helix loop helix family member a9)

DNA/RNA
Inip (INTS3 and NABP interacting protein)
TSEN34 (TRNA Splicing Endonuclease Subunit 34)
Rbfox1 (RNA binding protein fox1 homolog)
Tyw5 (tRNA-wybutosine synthesizing protein 5)
WBSCR27 (Williams–Beuren syndrome-related methyltransferase)
Atxn7l3 (Ataxin 7-like 3)
bHLHA9 (basic helix loop helix family member a9)
Neil 1 (Nei endonuclease VIII-like 1)
Zranb3 (zinc finger RNA-binding domain containing 3)
bHlha9 (basic helix loop helix family member a9)

Actin/Cytoskeleton
XIRP2 Xin actin-binding repeat-containing protein 2
Pdlim1 (PDZ and Lim domain 1)
Epb41l4a (erythrocyte membrane protein band 4.1 like 4a)
Abi3 (ABI gene family member 3)

Metabolism
Protein phosphatase 1E (PP2C domain containing) (PPM1E)
Aldolase A
Ptgs2 (Prostaglandin endoperoxide synthase 2)
HS3ST4 (Heparan sulfate-glucosamine 3-sulfotransferase 4)

Growth Factor
Lcn2 (lipocalin) neutrophil gelatinase-associated lipocalin (NGAL)
Flt1 (FMS-like tyrosine kinase 1)

Ubiquitination
Klhl3 (Kelch-like 3)
Atxn7l3 (Ataxin 7-like 3)

Neuronal Development
Robo3 (Roundabout guidance receptor 3)
Neil 1 (Nei endonuclease VIII-like 1)
Vwa1 (von Willebrand factor A domain containing 1)
Ptgs2 (Prostaglandin endoperoxide synthase 2)

Translation
Tsc1 (tuberous sclerosis 1)
RIOK2 (RIO Kinase 2)

Chaperone
Clgn (calmegin)

Extracellular Matrix
Vwa1 (von Willebrand factor A domain containing 1)

Endosomes
Clgn (calmegin)
Ccdc93 (coiled-coil domain containing 93)

Epigenetics
Atxn7l3 (Ataxin 7-like 3)
Tyw5 (tRNA-wybutosine synthesizing protein 5)

Autophagy
Dennd3 (DENN Domain Containing 3)
Tsc1 (tuberous sclerosis 1)

Inflammation
Lcn2 (lipocalin) neutrophil gelatinase-associated lipocalin (NGAL)
Ptgs2 (Prostaglandin endoperoxide synthase 2)

Ribosomes
RIOK2 (RIO Kinase 2)

Unknown Function
Fam163b
Mta3 (metastasis associated 3)
Predicted gene 5128(Gm5128)

Figure S3: Alcohol does not alter the transcription of Aldolase A, PPM1E and Rbfox2 in the NAc and protein level in the DLS

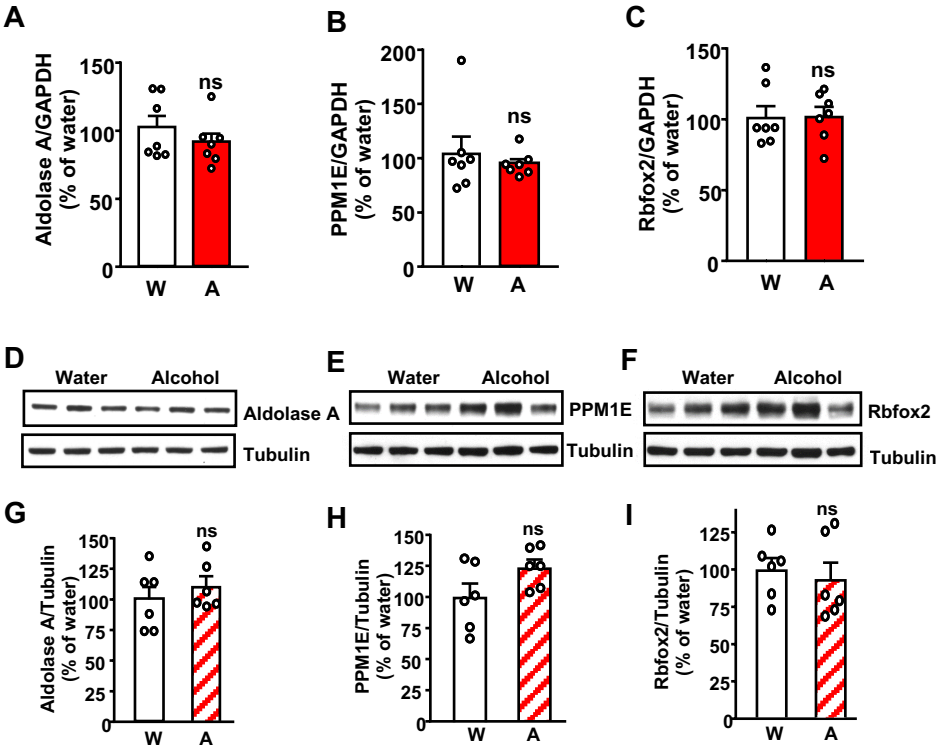

Figure S4: The levels of miR15b-5p, miR25-3p, miR92a-3p,and miR34a-5p are not altered by alcohol in the DLS

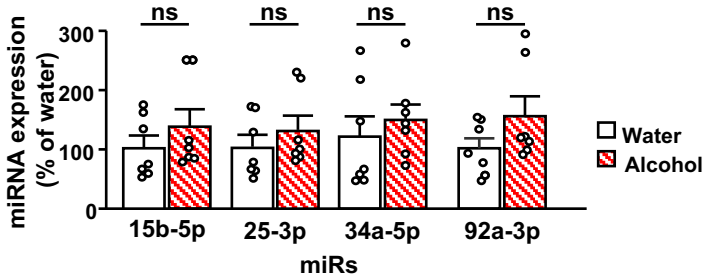

Figure S5: Alcohol does not alter the protein levels of Aldolase C in the NAc

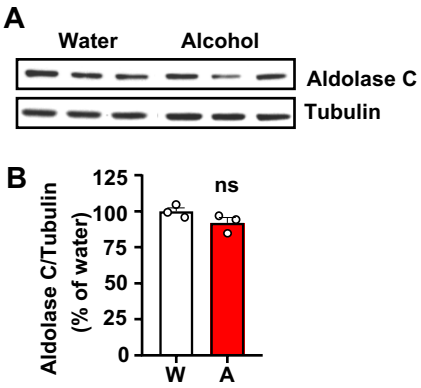

Figure S6: Alcohol does not affect the translation of the main glucose and lactate transporter in the NAc

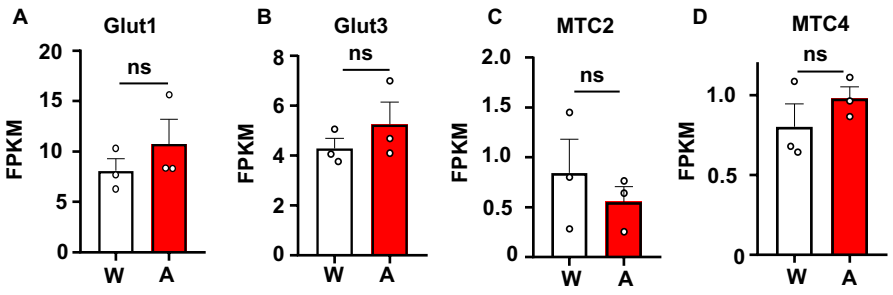

Figure S7: Blood glucose is unaltered by chronic alcohol drinking

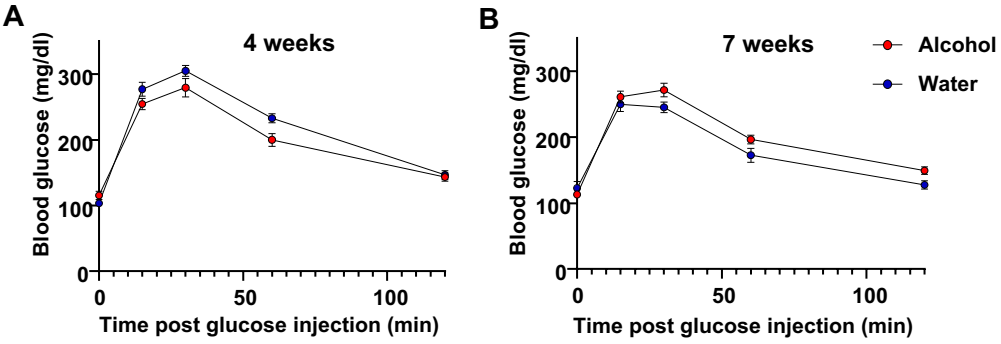

Figure S8: Subcutaneous administration of L-lactate does not affect locomotion

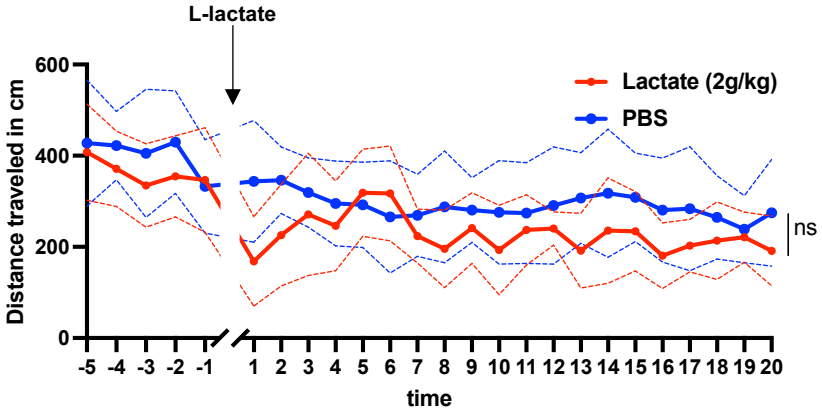

Figure S9: Subcutaneous administration administration of NaCl does not affect alcohol consumption

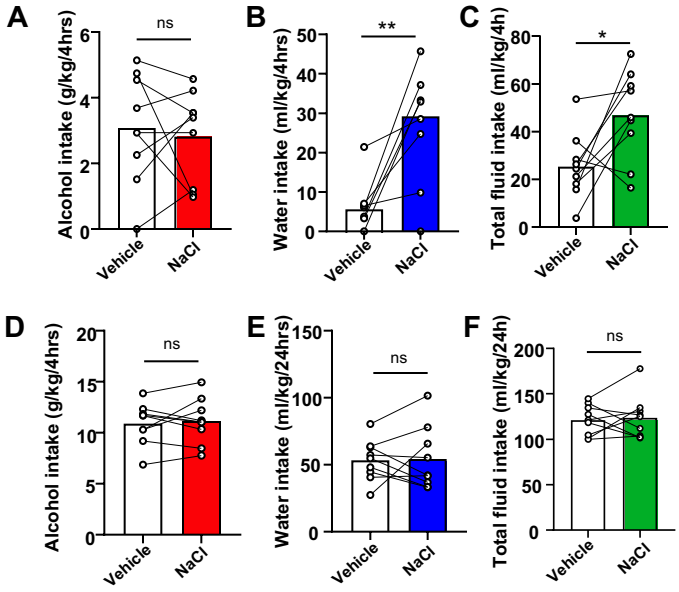

Figure S10: Subcutaneous administration administration of L-Lactate does not affect sucrose consumption

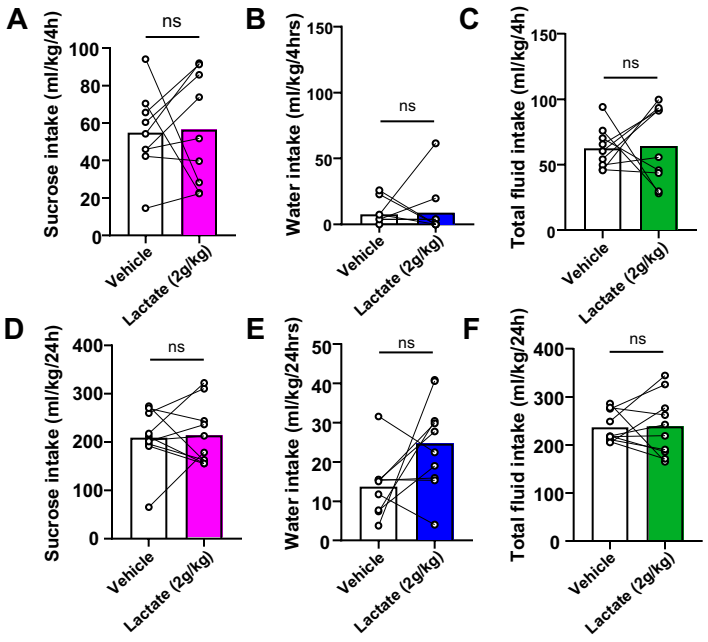

Table S1 Alcohol and sucrose drinking averages of mouse groups used in the study

Alcohol	Average Consumption (g/kg/24hr)	SEM (±g/kg/24hr)
1B-D and 2A-C	12.14	1.14
1E-H, 2D-I, S1C-F and S3D-I	12.52	1.63
S1A-B and S3A-C	13.60	0.96
3C-E	16.40	1.50
3G-L	17.89	1.47
4B and S4	13.25	0.97
4C-D	12.55	1.37
S5	14.18	1.35
6B	14.62	0.95
6C	11.30	0.87
S7	12.80	2.11
7B-G and S9	10.88	2.62
Sucrose	**Average Consumption (ml/kg/24hr)**	**SEM (±ml/kg/24hr)**
S10	213.56	21.07

Table S2 Statistical analyses of the data

	Group Size	Statistical Test	Main effect	t- or f-statistic	p-value	Post-hoc	Post-hoc comparison	p-value
Figure 1B	n=5 per group	Two-way ANOVA	Alcohol x Rapamycin	F(1,16)=13.86	p=0.0019	Tukey's test	water and alcohol within the vehicle group	p=0.0008
			Alcohol	F(1,16)=10.23	P=0.0056		vehicle and rapamycin within the alcohol group	p=0.0014
			Rapamycin	F(1,16)=7.957	P=0.0123			
Figure 1C	n=5 per group	Two-way ANOVA	Alcohol x Rapamycin	F(1,16)=6.541	p=0.0211	Tukey's test	water and alcohol within the vehicle group	p=0.0137
			Alcohol	F(1,16)=5.84	P=0.0280		vehicle and rapamycin within the alcohol group	p=0.0165
			Rapamycin	F(1,16)=5.224	P=0.0363			
Figure 1D	n=5 per group	Two-way ANOVA	Alcohol x Rapamycin	F (1, 16) = 2.198	P=0.1576			
			Alcohol	F(1,16)=0.1552	p=0.6989			
			Rapamycin	F(1,16)=0.0019	p=0.9656			
Figure 1G	n=8 per group	Unpaired t-test		t(14)=4.354	p=0.0007			
Figure 1H	n=8 per group	Unpaired t-test		t(14)=4.354	p=0.0007			
Figure 2A	n=5-6 per group	Two-way ANOVA	Alcohol x Rapamycin	F(1,16)=18.01	p=0.0006	Tukey's test	water and alcohol within the vehicle group	p=0.0001
			Alcohol	F(1,16)=16.38	P=0.0009		vehicle and rapamycin within the alcohol group	p=0.0001
			Rapamycin	F(1,16)=15.56	P=0.0012			
Figure 2C	n=5-6 per group	Two-way ANOVA	Alcohol x Rapamycin	F(1,16)=12.86	p=0.0025	Tukey's test	water and alcohol within the vehicle group	p=0.001
			Alcohol	F(1,16)=10.51	P=0.0051		vehicle and rapamycin within the alcohol group	p=0.0002
			Rapamycin	F(1,16)=19.13	P=0.0005			
Figure 2D	n=5-6 per group	Two-way ANOVA	Alcohol x Rapamycin	F(1,16)=27.39	p<0.0001	Tukey's test	water and alcohol within the vehicle group	p<0.0001
			Alcohol	F(1,16)=18.9	P=0.0005		vehicle and rapamycin within the alcohol group	p<0.0001
			Rapamycin	F(1,16)=11	P=0.0044			
Figure 2G	n=8 per group	Unpaired t-test		t(14)=4.413	p=0.0006			
Figure 2H	n=8 per group	Unpaired t-test		t(14)=5.426	p<0.0001			
Figure 2I	n=8 per group	Unpaired t-test		t(14)=2.917	p=0.0113			
Figure 3D	n=3 per group	Unpaired t-test		t(4)=27.29	p=<0.0001			
Figure 3G	n=9-10 per group	Unpaired t-test		t(17)=4.042	p=0.0008			

Figure 3H	n=9-10 per group	Unpaired t-test		t(17)=2.575	p=0.0197			
Figure 3I	n=9-10 per group	Unpaired t-test		t(8)=2.322	p=0.0488			
Figure 3J	n=9-10 per group	Unpaired t-test		t(17)=2.299	p=0.0345			
Figure 3K	n=9-10 per group	Unpaired t-test		t(17)=3.425	p=0.0032			
Figure 3L	n=9-10 per group	Unpaired t-test		t(17)=4.26	p=0.0005			
Figure 4B	n=7 per group	Two-way ANOVA	Alcohol x miR	F (5, 72) = 8.224	P<0.0001	Sidak's test	miR15b-5p water vs alcohol	p=0.0012
			Alcohol	F(1,72)=50.37	p<0.0001		miR 25-3p water vs alcohol	p=0.0045
			miR	F(5,72)=5.102	P=0.0005		miR 34a-5p water vs alcohol	p<0.0001
							miR 92a-3p water vs alcohol	p<0.0001
							miR 127-3p water vs alcohol	p=0.9549
							miR 34a-3p water vs alcohol	p=0.9994
Figure 4C	n=5-6 per group	Two-way ANOVA	Alcohol x Rapamycin	F(1,17)=7.291	p=0.0152	Sidak's test	water and alcohol within the vehicle group	p=0.0189
			Alcohol	F(1,17)=5.107	P=0.0372		vehicle and rapamycin within the alcohol group	p=0.0366
			Rapamycin	F(1,17)=2.621	P=0.1238			
Figure 4D	n=5-6 per group	Two-way ANOVA	Alcohol x Rapamycin	F(1,17)=0.01218	P=0.9134			
			Alcohol	F(1,17)=2.866	P=0.1087			
			Rapamycin	F(1,17)=0.002773	P=0.9586			
Figure 5C	n=4 of independent replicates	Two-way ANOVA	miR vs. Aldolase A 3'UTR	F(2,18)=7.882	p=0.0035	Sidak's test	Aldolase A 3'UTR alone vs. Aldolase A 3'UTR + miR34a-5p	p=0.0001
			Aldolase A 3'UTR	F(1,18)=3.144	P=0.0931		Aldolase 3'UTR + miR34a-5p vs. Aldolase A 3'UTR + miR control	p<0.0001
			miR	F(2,18)=34.75	P<0.0001		Aldolase A 3'UTR mutant + miR34a-5p vs. Aldolase A 3'UTR + miR34a-5p	p=0.007
							Aldolase A 3'UTR + miR34a-5p vs. Aldolase A 3'UTR mutant + miR control	p<0.0001
Figure 5F	n=4-5 per group	Mann-Whitney test		U=0	p=0.0159			
Figure 6B	n= 6-7 per group	Mann-Whitney tests		Lactate U=4	p=0.0140			
				Citrate U=6	p=0.035			

				a-Ketogluturate U=6	p=0.035			
				Malate U=3	p=0.0082			
Figure 6C	n=6 per group	One-way ANOVA		F(2,15)=13.48	p=0.0004	Tukey's test	water/vehicle vs alcohol/vehicle	p=0.0005
							alcohol/vehicle vs alcohol/rapamycin	p=0.004
Figure 7A	n=4-5 per group	Two-way ANOVA	miR34a-5p overexpression x Time	F(5, 32) = 0.4538	p=0.8074			
			miR34a-5p overexpression	F(1,7)=6.150	p=0.0422			
			Time	F(2.032,13.00)=1.798	p=0.2042			
Figure 7B	n=9 per group	Paired t-test		t(8)=7.562	p<0.0001			
Figure 7C	n=9 per group	Paired t-test		t(8)=5.917	p=0.0004			
Figure 7D	n=9 per group	Paired t-test		t(8)=4.742	p=0.0015			
Figure 7E	n=9 per group	Paired t-test		t(8)=2.004	p=0.08			
Figure 7F	n=9 per group	Paired t-test		t(8)=2.352	p=0.0509			
Figure 7G	n=9 per group	Paired t-test		t(8)=1.316	p=0.2297			
Figure S1A	n=7 per group	Mann-Whitney test		U=18	p=0.4557			
Figure S1B	n=7 per group	Mann-Whitney test		U=17	p=0.3829			
Figure S1E	n=5-6 per group	Mann-Whitney test		U=16	p=0.8182			
Figure S1F	n=5-6 per group	Mann-Whitney test		U=12	p=0.6623			
Figure S3A	n = 7 per group	Mann-Whitney test		U=19	p=0.535			
Figure S3B	n = 7 per group	Mann-Whitney test		U=22	p=0.8048			
Figure S3C	n = 7 per group	Mann-Whitney test		U=22	p=0.8048			
Figure S3G	n=6 per group	Mann-Whitney test		U=13	p=0.4848			
Figure S3H	n=6 per group	Mann-Whitney test		U=8	p=0.132			
Figure S3I	n=6 per group	Mann-Whitney test		U=14	p=0.5887			
Figure S4	n = 7 per group	Two-way ANOVA	Alcohol x miR	F (3, 48) = 0.1223	P=0.9465	Sidak's test	miR15b-5p water vs alcohol	p=0.8127
			Alcohol	F (1, 48) = 4.160	P=0.0469		miR 25-3p water vs alcohol	p=0.9047
			miR	F (3, 48) = 0.2028	P=0.8939		miR 34a-5p water vs alcohol	p= 0.8868
							miR 92a-3p water vs alcohol	p=0.4289
Figure S5	n=3 per group	Mann-Whitney test		U=1	p=0.2			

Figure S7A	n=6-12 per group	Two-way ANOVA	Alcohol x Time	F(4,64)=2.232	p=0.0753			
			Alcohol	F(1,16)=2.397	p=0.1411			
			Time	F(3.001,48.02)=158.3	p<0.0001			
Figure S7B	n=6-12 per group	Two-way ANOVA	Alcohol x Time	F(4,64)=1.911	p=0.1193			
			Alcohol	F(1,16)=3.159	p=0.0945			
			Time	F(2.898,46.36)=148.8	p<0.0001			
Figure S8	n=9	Two-way RM ANOVA	Lactate x Time	F (19, 160) = 1.250	P=0.2247			
			L-lactate	F (19, 160) = 0.9351	P=0.5409			
			Time	F (1, 160) = 39.64	P<0.0001			
Figure S9A	n=9 per group	paired t-test		t(8)=0.4397	p=0.6718			
Figure S9B	n=9 per group	paired t-test		t(8)=4.204	p=0.003			
Figure S9C	n=9 per group	paired t-test		t(8)=2.613	p=0.031			
Figure S9D	n=9 per group	paired t-test		t(8)=0.5005	p=0.6302			
Figure S9E	n=9 per group	paired t-test		t(8)=0.1377	p=0.8938			
Figure S9F	n=9 per group	paired t-test		t(8)=0.3203	p=0.7569			
Figure S10A	n=9 per group	paired t-test		t(8)=0.1349	p=0.8960			
Figure S10B	n=9 per group	paired t-test		t(8)=0.1971	p=0.8482			
Figure S10C	n=9 per group	paired t-test		t(8)=0.1370	p=0.8944			
Figure S10D	n=9 per group	paired t-test		t(8)=0.2076	p=0.8402			
Figure S10E	n=9 per group	paired t-test		t(8)=1.827	p=0.1051			
Figure S10F	n=9 per group	paired t-test		t(8)=0.4631	p=0.6556			

Table S3: Alcohol via mTORC1 decreases the translation of transcripts in the NAc

Gene ID	Gene Accession Number	Gene Name	Folds Alcohol	p value Alcohol	Folds Rapamycin	p value Rapamycin
Vwa1	NM_147776	von Willebrand factor A domain containing 1	-0.602	0.016	0.614	0.04
Dennd3	NM_001081066	DENN domain-containing protein 3	-0.589	0.002	0.655	0.039
Igtp	NM_018738	interferon gamma induced GTPase	-0.571	0.006	0.511	0.02
Riok2	NM_025934	RIO kinase 2	-0.563	0.038	0.489	0.024
Aldoa	NM_001177307	aldolase A	-0.557	0.022	0.716	0.038
Ptgs2	NM_011198	prostaglandin endoperoxide synthase 2	-0.55	0.031	0.664	0.045
Bhlha9	NM_177182	basic helix loop helix family member a9	-0.545	0.017	0.702	0.015
Gm5128	NM_183320	predicted gene 5128	-0.53	0.025	0.618	0.053
Hs3st4	NM_001252072	heparan sulfate 3-O-sulfotransferase 4	-0.506	0.008	0.403	0
Abi3	NM_025659	ABI gene family member 3	-0.467	0.014	0.368	0.03
Atxn7l3	NM_001098836	ataxin 7-like 3	-0.467	0.038	0.357	0.006
Mta3	NM_054082	metastasis associated 3	-0.465	0.014	0.503	0.03
Tsc1	NM_022887	tuberous sclerosis 1	-0.453	0.032	0.424	0.033
Neil 1	NM_028347	nei endonuclease VIII-like 1	-0.422	0.032	0.462	0.02
Robo3	NM_001164767	roundabout guidance receptor 3	-0.417	0.022	0.609	0.024
Pde4dip	NM_001039376	phosphodiesterase 4D interacting protein	-0.394	0.047	0.341	0.011
Ppm1e	NM_177167	protein phosphatase 1E	-0.386	0.054	0.658	0.004
Wbscr27	NM_024479	Williams Beuren syndrome chromosome region 27	-0.376	0.018	0.361	0.011
Clgn	NM_009904	calmegin	-0.376	0.018	0.418	0.034
Zranb3	NM_027678	zinc finger RNA-binding domain containing 3	-0.362	0.02	0.423	0.032
Tyw5	NM_001037742	tRNA-yW synthesizing protein 5	-0.35	0.034	0.316	0.019
Flt1	NM_010228	FMS-like tyrosine kinase 1	-0.315	0.01	0.41	0.047
Fam163b	NM_175427	protein fam163b	-0.286	0.001	0.307	0.047
Ccdc93	NM_001025156	coiled-coil domain containing 93	-0.23	0.012	0.224	0.03
Epb41l4a	NM_013512	erythrocyte membrane protein band 4.1 like 4a	-0.213	0.04	0.246	0.047
Pdlim1	NM_016861	PDZ and Lim domain 1	-0.206	0.021	0.235	0.031
Rbfox2	NM_175387	RNA binding protein fox1 homolog	-0.182	0.018	0.199	0.041
Tsen34	NM_001164204	tRNA splicing endonuclease subunit 34	-0.181	0.013	0.268	0.015
Xirp2	NM_001083919	xin actin binding repeat containing 2	-0.169	0.004	0.459	0.034
Lcn2	NM_008491	lipocalin	-0.165	0.019	0.087	0.036
Inip	NM_001013577	INTS3 and NABP interacting protein	-0.152	0.012	0.169	0.005
Klhl3	NM_001195075	kelch-like protein 3	-0.062	0.023	0.084	0.041